

Transport properties in small-scale coastal flows: relative dispersion from VHF radar measurements in the Gulf of La Spezia

Angelique C. Haza · Tamay M. Özgökmen ·
Annalisa Griffa · Anne Molcard ·
Pierre-Marie Poulain · Germana Peggion

Received: 8 November 2009 / Accepted: 11 May 2010 / Published online: 6 June 2010
© Springer-Verlag 2010

Abstract Lagrangian transport characteristics in the Gulf of La Spezia, a 5×10 -km area along the western coast of Italy, are investigated using data collected from a very high frequency (VHF) radar system with 250 m and 30-min resolution and two clusters of Coastal Dynamics Experiment surface drifters during 2 weeks in the summer of 2007. The surface drifters are found to follow the temporal and spatial evolution of the finite-scale Lyapunov exponents (FSLEs) computed by the VHF radar, indicating the precision of both the radar measurements and the diagnostic FSLE in mapping accurately the transport pathways. In light of this agreement, an analysis of the relative dispersion is conducted. It is found that the average FSLE value varies within a narrow range of $4 \text{ day}^{-1} \leq \lambda \leq 7 \text{ day}^{-1}$ and displays an exponential regime over the entire extent of the measurements. The dynamical implication is that relative dispersion is controlled nonlocally, namely by slow, persistent, energetic mesoscale structures as

opposed to the rapidly evolving high-gradient small-scale turbulent features. The value of the exponent is about an order of magnitude larger than those found in previous modeling studies and analysis of SCULP data in the Gulf of Mexico but somewhat smaller than that estimated from CLIMODE drifters in the Gulf Stream region. Scaling of the FSLE using a metric of resolved gradients of the Eulerian fields in the form of a positive Okubo–Weiss criterion is useful, but not as precise as in modeling studies. The horizontal flow convergence is found to have a small yet tangible effect on relative dispersion.

Keywords Relative dispersion · FSLE · Lagrangian coherent structures · VHF radar · Coastal turbulence

1 Introduction

Being able to monitor and predict the coastal ocean circulation and the associated transport is of great relevance for a correct management of the coastal ecosystem. Coastal currents advect ecologically relevant quantities such as larvae and phytoplankton and directly influence the ecosystem through variations of physical quantities such as temperature. Also, the knowledge of the coastal currents and transport is crucial in case of accidents at sea, for instance to guide operations for damage control in case of discharges of pollutants. In order to tackle these types of problems properly, one needs to solve

$$\frac{d\mathbf{x}}{dt} = \mathbf{v}(t) = \mathbf{u}(\mathbf{x}, t), \quad (1)$$

Responsible Editor: Pierre De Mey

A. C. Haza · T. M. Özgökmen (✉) · A. Griffa
RSMAS/MPO, University of Miami, Miami, FL, USA
e-mail: tozgekmen@rsmas.miami.edu

A. Griffa
ISMAR-CNR, La Spezia, Italy

A. Molcard
LSEET, University of Toulon, Toulon, France

P.-M. Poulain
OGS, Trieste, Italy

G Peggion
University of Southern Mississippi, Hattiesburg, MS, USA

where \mathbf{x} represents the 3-D (or 2-D) positions of Lagrangian particles, \mathbf{v} is the Lagrangian velocity, and \mathbf{u} is the Eulerian velocity field.

Despite this simple equation, there are fundamental difficulties in establishing the relationship between Lagrangian trajectories and the underlying flow field for typical oceanic applications. First, $\mathbf{u}(\mathbf{x}, t)$ is usually very challenging to measure and as such not accurately known. This is because of the large range of scales of oceanic flows, or more formally the high Reynolds number. Using a characteristic coastal speed scale $U \approx 10^{-1} \text{ ms}^{-1}$, length scale $L \approx 10^3 \text{ m}$, and kinematic viscosity $\nu = 10^{-6} \text{ m}^2 \text{ s}^{-1}$, a typical estimate can be obtained as $Re = UL/\nu \approx 10^8$. If these coastal flows are to display classical 3-D, homogeneous, isotropic turbulent cascade, then the number of degrees of freedom can be estimated by $Re^{9/4}$ (Lesieur 1997), and we obtain $\approx O(10^{18})$ as the number of spatial sampling point needed for unit time. Clearly, this is a very large number in the context of the present observing systems. The ocean may not always exhibit classical 3-D turbulent energy cascade over a wide wavenumber range. This is not only because both rotation (by favoring inverse energy cascade) and stratification (by limiting vertical motions) act to reduce the number of degrees of freedom but also sustained turbulence requires sustained forcing, and such forcing may not exist at all places continuously. Indeed, in many instances, the ocean state appears dominated by so-called turbulent coherent structures, by which we refer to features such as jets, eddies, and filaments that, once created by various instabilities, contain the most kinetic energy and exhibit a slow decay in the flow field. Even though this implies a reduced number of degrees of freedom to be resolved, the presence of coherent structures does not necessarily ease the difficulties in predicting transport and dispersion since their fundamental nature remains not well understood. In particular, their time variability, even though slow, may dictate much of the transport characteristics so that any errors in the estimation of the details of turbulent coherent structures can propagate directly into trajectory calculations. Also, the time variability of these coherent structures can cause Lagrangian trajectories to be chaotic, further enhancing the difficulty in transport prediction (Aref 1984). Detection and prediction of coherent structure variability is complex since it could be associated with the inherent variability of the turbulent flows as well as with external (e.g., wind) forcing.

In the light of these challenges, two complementary methods are typically used for practical problems involving Lagrangian dynamics in oceanic flows. The first one is a statistical approach, which has been pi-

oneered for oceanic applications by Griffa (1996). In this method, the Lagrangian velocity is decomposed into a mean and eddy component, similar to what is done in Reynolds decomposition. The mean flow incorporates some basic turbulent coherent structures, such as boundary currents, meandering jets, and gyres, while the eddy component is modeled as a Markov process satisfying the so-called Langevin equation. The net effect of turbulent interactions is modeled as a diffusive process, and the eddy velocities can also have a memory time scale. An important step in the use of such models is the estimation of the parameters from existing drifter data sets (Davis 1991; Fratantoni 2001; Richardson 2001; Bauer et al. 2002). This approach has shown much promise in estimating the envelope of oceanic Lagrangian motion (Falco et al. 2000). Further details of turbulent coherent structures, in particular the trapping effect of mesoscale eddies, can be incorporated in these models (Veneziani et al. 2005a, b), as well as other details can be represented by higher-order models of Lagrangian eddy velocity (Berloff and McWilliams 2002). Prediction of individual trajectories has been attempted by assimilating nearby particle positions into these Lagrangian models (Özgökmen et al. 2000, 2001; Castellari et al. 2001). The main advantage of this approach is that it inherently takes into account some of the uncertainties in the estimation of Eulerian velocity field and turbulent interactions, and the models are simple, easily relocatable, and can provide a faithful reproduction of the Lagrangian motion in a statistical sense. Once the parametric model is developed for a certain region, they can also be useful for prognostic purposes. Their main drawback is that, since the flow field is represented in several parameterized components (mean, mesoscale eddy, and turbulence), they may not provide dynamical insight in the presence of flows with complex spatial structure and temporal variability, such as in small-scale coastal flows, the characteristics of which may not be quite consistent with the assumptions made in these models.

A different, namely deterministic approach is the use of dynamical system concepts under the assumption that the time evolution of the Eulerian velocity field is fully known and that transport is mostly controlled by mesoscale turbulent structures. The key concept here is hyperbolicity induced by turbulent coherent structures that create directions in which stretching can cause particles to diverge from the structures along so-called unstable manifolds as well as to converge along stable manifolds (Ottino 1989). The stable and unstable manifolds intersect at so-called hyperbolic trajectories, the motion of which is central to the understanding of the effect of time dependence on the pathways of

Lagrangian particles. There has been a rapid development of these techniques (Wiggins 2005). In particular, the initial restriction to periodic, infinite-time systems has been overcome by focusing on transient stagnation points, finite-time analogs of stable and unstable manifolds, and analysis of finite-time data (Haller and Poje 1998; Poje and Haller 1999; Coulliette and Wiggins 2000; Miller et al. 2002). These techniques have been useful in the improvement of the reconstruction of Eulerian fields from Lagrangian data (Poje et al. 2002; Toner and Poje 2004) and in the performance of a Lagrangian data assimilation scheme (Molcard et al. 2006). Lagrangian coherent structures (LCS) such as stable and unstable manifolds and hyperbolic trajectories help visualize the combined effect of the time variability and geometric features (such as eddies and jets) on transport. Common methods to compute LCS include finite-scale Lyapunov exponent (FSLE; Artale et al. 1997; Aurell et al. 1997) in which the hyperbolicity is estimated on the basis of relative dispersion, namely how fast particle pairs separate from an initial distance of δ to $\alpha\delta$, where α is a specified factor. A similar metric is the finite-time Lyapunov exponent (FTLE; Haller 1997). Lagrangian analysis of oceanic fields using FSLE and FTLE is being widely used (d'Ovidio et al. 2004; Olascoaga et al. 2006; Haza et al. 2007, 2008; Shadden et al. 2008; Poje et al. 2010). The primary advantage of this approach is that it requires no assumptions or parameterizations of the nature of oceanic turbulence, while permitting investigation of Lagrangian motion in flow fields with complex spatial and temporal dependence. Nevertheless, these are essentially diagnostic methods requiring full knowledge of the oceanic velocity field, either from satellite altimeter data, numerical models, or coastal measurements. The spatial resolution of these data sets is typically on the order of 100 km for satellite altimeters, 1 to 10 km for models, and few kilometers to few hundred meters for coastal radar measurements, exhibiting spatial gaps that could create significant uncertainties.

Given that particle motion is sensitive to all scales and oceanic Lagrangian instruments experience forces imparted at their own scale, namely $O(1)$ m, one of the next frontiers is the development of a better understanding of the effect of unresolved scales of motion on Lagrangian transport. It has been put forth that geostrophically balanced, mesoscale oceanic flows are largely nondissipative, due to backward energy cascade from smaller to larger scales (McWilliams 1985, 2003). Therefore, only a loss of balance can create a circumstance leading to injection of energy to smaller scales via a forward energy cascade (Molemaker and McWilliams 2005). So-called submesoscale instabilities

that can establish a pathway to small-scale motions have been modeled in the context of surface mixed layers (Mahadevan 2006; Boccaletti et al. 2007). However, it is not known whether such instabilities covering a wide spectrum of scales are typical or occur only sporadically in the ocean (Griffa et al. 2008). Therefore, the fundamental question that needs to be addressed is whether it is the slow, persistent, energetic mesoscale structures or the rapidly evolving small-scale structures that control the main transport and dispersion in the ocean.

One of the ways to address this question is via the simultaneous availability of Eulerian velocity fields and Lagrangian particle trajectories. The availability of high-resolution real-time measurements of near-surface velocity field from high frequency (HF) and very high frequency (VHF) radars is emerging as one of the most suitable avenues to make progress in this area. HF radars operate in a frequency range of 12–30 MHz with associated range of 40–100 km and space resolution of several kilometers, while VHF radars configured in a frequency range of 40–50 MHz can resolve the motion at several hundreds of meters, thereby providing information on both submesoscale and mesoscale flows. Quantitative assessments of radar velocity measurements have been provided by a number of studies, comparing radar results with in situ measurements from various platforms such as moored current meters, ADCP profilers, and drifters (Steward and Joy 1974; Schott et al. 1986; Shay et al. 1998a, b, 2001, 2007; Paduan and Rosenfeld 1996; Kaplan et al. 2005; Paduan et al. 2006).

Of particular interest here are studies based on the simultaneous availability of HF radar derived velocity fields and Lagrangian drifters. The evaluation conducted by Ullman et al. (2006) using HF radar and drifters on the New Jersey shelf indicates that subgrid-scale fluctuations seem to be suitable for parameterizations using the Lagrangian stochastic models put forth by Griffa (1996). Ohlmann et al. (2007) employed repeated releases of about a dozen of drifters within the HF radar field off the Santa Barbara and San Diego coasts and found root mean square (rms) differences of the radial velocities between HF radar and drifters mostly within the range of 3 to 5 cm s^{-1} . Nevertheless, errors reaching 20 cm s^{-1} were also encountered for individual drifter comparison. Differences of such magnitude indicate the presence of significant subgrid-scale motions. Shadden et al. (2008) used LCS computed from HF radar velocity fields in Monterey Bay and found that the fate of the observed drifter motion is better characterized based on the LCS than a direct interpretation of current data.

In this paper, we consider a significantly smaller-scale coastal flow recently measured by VHF radar and drifters. The region of interest is the Gulf of La Spezia in the northwestern Mediterranean Sea, where a WERA radar was operated at a frequency of 45.25 MHz (with a 500-KHz bandwidth) with a spatial resolution of 250 m during the period 15–30 June 2007 in the framework of the LASIE/POET experiment (Molcard et al. 2009). The radar data have been compared with surface drifter data launched in clusters (Molcard et al. 2009), showing differences of approximately 5 cm s^{-1} in speed and absolute dispersion of 1 km every 12 h, which are on the low side of the errors reported in the literature. The velocity field, typical of small and protected areas, is characterized by relatively low values (rms speeds of approximately 8 cm s^{-1}) and by complex patterns and high temporal variability (order of hours). Specifically, we are interested in making progress in addressing the following questions:

- Do LCS, quantified by the FSLEs computed from VHF-derived velocity fields, provide an accurate indication of the observed drifter motion in small-scale coastal flows, or there are deviations indicating significant subgrid-scale motions?
- What are the characteristics of turbulent coherent structures in this coastal flow? Are there any indications of turbulent breakdown of mesoscale eddies, or the flow is mainly driven by external forcing events?

- What are the main characteristics of relative dispersion in such flows? Are they mostly controlled by turbulent coherent structures or are there any indications that the small scales exert a significant effect on the spreading?
- Do other small-scale coastal effects, such as divergence and convergence zones, play an important role in controlling particle motion?

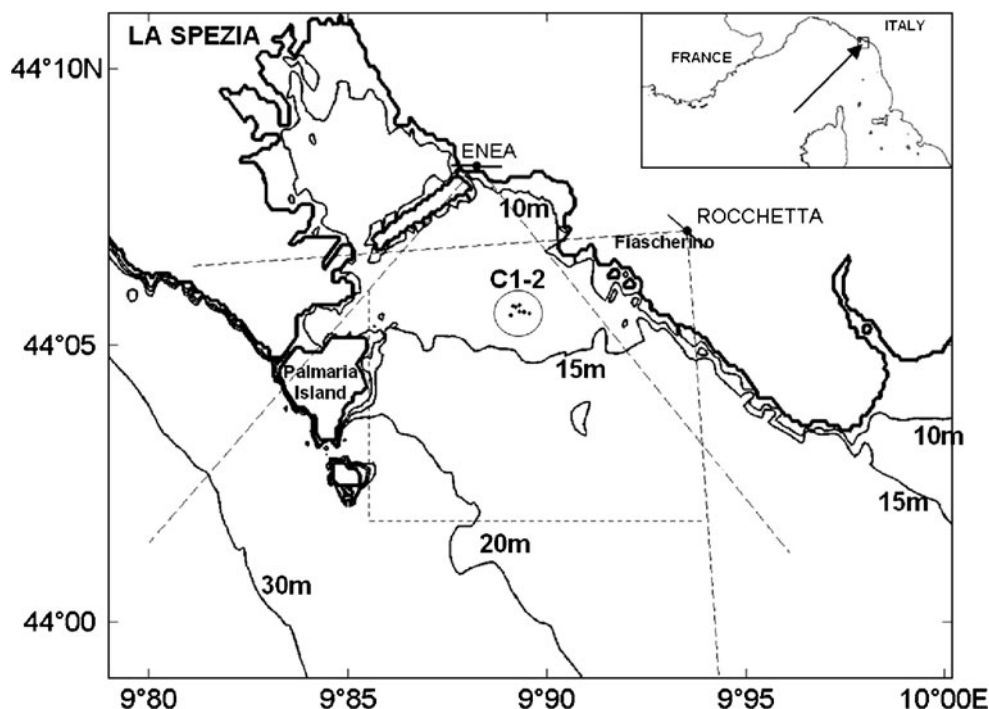
Answers to such questions are likely to be relevant for both a better understanding of coastal ocean dynamics over a wider range of scales and the practical applications of VHF radar derived velocity fields for transport prediction.

2 Area of interest and data sets

2.1 Characteristics of the area of interest

The area of interest is the Gulf of La Spezia situated in the Ligurian Sea in the northwestern Mediterranean Sea (Fig. 1). The coastal observations studied here have been collected within the framework of the Ligurian Sea Marine Rapid Environment Assessment experiment, MREA07, and in particular during the POET-LASIE component (Gasparini et al. 2009) in the Gulf of La Spezia during the period June 15–30 2007. The Gulf is a highly anthropized area characterized by a complex use of the land, where monitoring and prediction of

Fig. 1 The coverage of VHF radars from ENEA and ROCCHETTA stations and the initial launch location (marked as C1-2) in the Gulf of La Spezia. The inset shows the geographical location of the Gulf along the western Italian coast



coastal currents and transport is expected to play an important role for a correct coastal management. The Gulf is oriented along northwest and southeast, and it is approximately 5 km wide and 10 km long with respect to these directions.

The dynamics of the Gulf are quite complex due to a number of reasons. First, the circulation in the Gulf is influenced by the larger-scale Ligurian current (Gasparini et al. 2009; Molcard et al. 2009), which is characterized by a cyclonic boundary current flowing along the Italian coast, modulated by seasonality and wind forcing (Astraldi et al. 1990). The winds during summer are predominantly from the south (Bordone and Lisca 2009). Southeasterly wind (Sirocco) is downwelling prone and tends to reinforce the cyclonic circulation while southwesterly wind (Libeccio) is more disruptive of the circulation. During the LASIE-POET experiments, three main wind episodes occurred: a Sirocco episode during June 18–19 and two Libeccio events during June 22–23 and 26–27, separated by periods with weaker and more disorganized winds. The response of the Ligurian current to the wind is depicted by the results of the Navy Coastal Ocean Model (NCOM) model (Martin 2000) that has been run in real time by the Naval Research Laboratory (NRL) during the MREA07 experiment (Vandenbulcke et al. 2009). The NRL prediction system is based on the relocatable version of NCOM, and it was configured with three nesting domains at resolutions of 4, 2, and 0.6 km, respectively, and forced by the COAMPS winds and NOGAPS0.5 thermal forcings. The outer most nest is coupled with NCOM configured on a global scale at a $1/8^\circ$ resolution which is operational at NAVO (http://www7320.nrlssc.navy.mil/global_ncom/index.html). While the NCOM simulations cannot capture accurately the detailed velocity fields inside the Gulf due to lack of resolution and details of forcing, they provide the larger-scale context surrounding the Gulf.

Here, we illustrate the current response to wind focussing on the period June 18–20, during which radar and drifter data are available and that is extensively analyzed in Section 3. Daily average currents from NCOM in the Ligurian Sea region surrounding the Gulf are shown in Fig. 2 and large-scale winds from QuickSCAT are shown in Fig. 3a, b for the days 18 and 20. During June 18, Sirocco winds are evident, blowing consistently northwestward along the Italian west coast and inducing a strong and well-organized Ligurian Sea boundary current hugging the coast (Fig. 2a). By June 20, the Sirocco episode has significantly subsided, and the corresponding Ligurian current appears less organized and situated far away

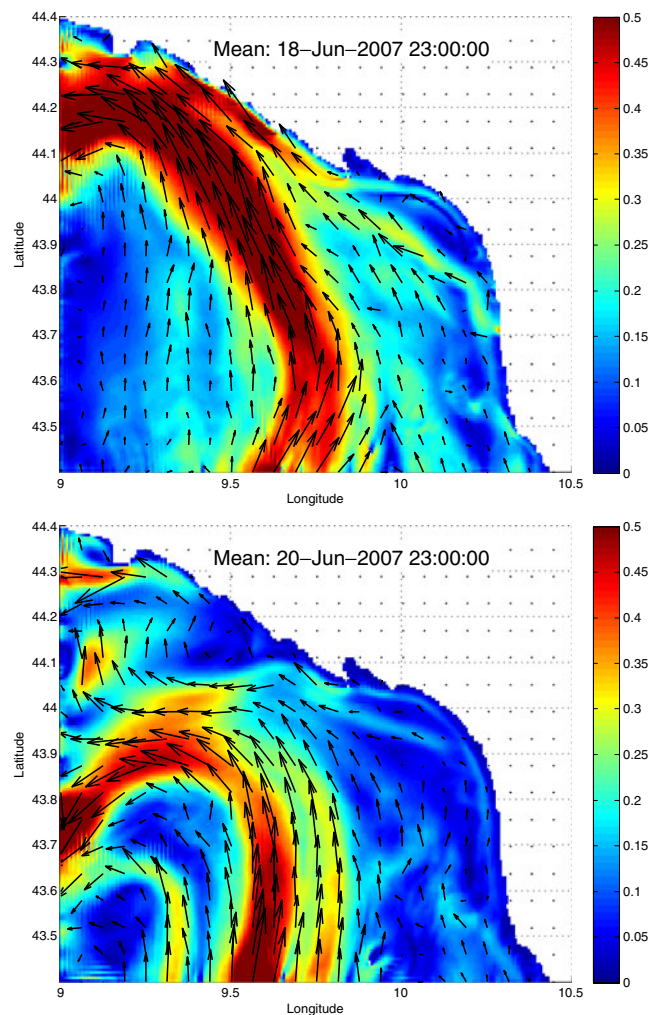


Fig. 2 A numerical simulation with the NCOM showing the larger-scale circulation in the eastern Ligurian Sea during the time frame coinciding with the POET-LASIE experiment. Surface velocity fields corresponding to the daily-average (*upper panel*) on 18 June 2007, in which scirocco (southeasterly) wind dominated, and (*lower panel*) on 20 June 2007, in which the wind was weaker and less coherent. Color bar indicates speed in meters per second

from the coast (Fig. 2b). Disorganized patterns and a further weakened circulation are observed during the following Libeccio episodes (not shown).

Inside the Gulf, a detailed analysis of the recent hydrographic observations indicates that a cyclonic current tends to generally exist (Fig. 12 of Gasparini et al. 2009). When the Ligurian current is stronger and closer to the coast, as during Sirocco, also the cyclonic circulation inside the Gulf is reinforced. When instead the Ligurian current is weaker and less organized, as in the periods of weak large-scale winds or during Libeccio, the dynamics of the Gulf tend to exhibit a greater

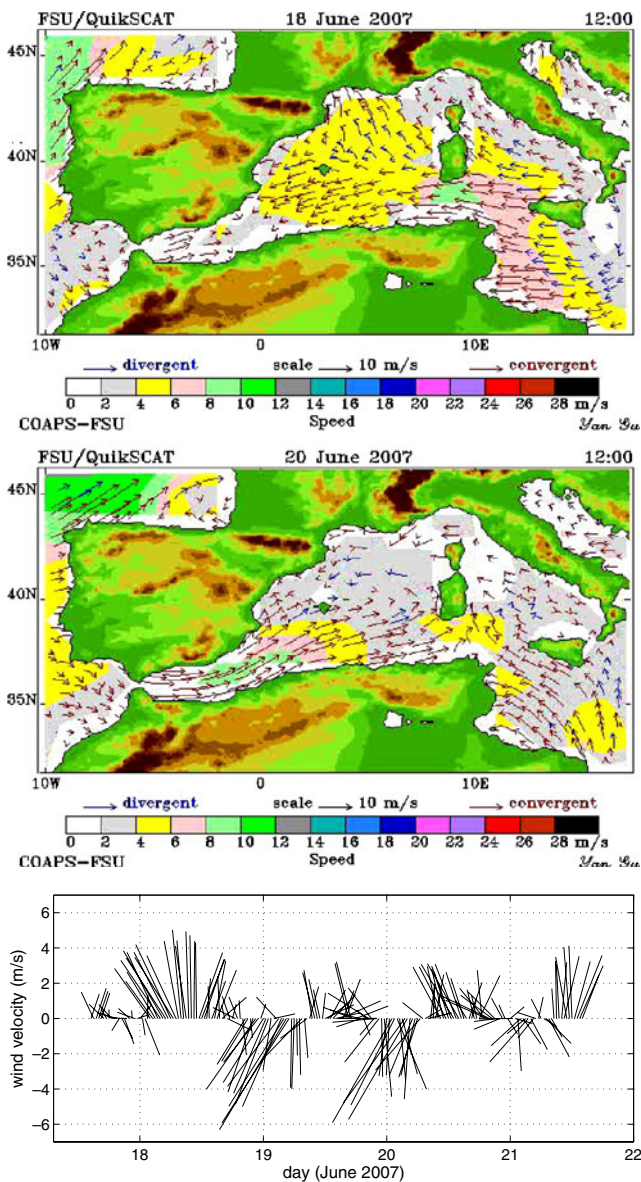


Fig. 3 Large-scale winds estimated by QuickSCAT for the Mediterranean basin during periods corresponding to launches of the two clusters (*upper and middle panels*). Time evolution of the local wind velocity observed at the Enea (see Fig. 1) station (*lower panel*)

degree of spatial and temporal variability and the local forcing needs to be considered.

The Gulf is surrounded by a complex orography that significantly influences the local winds. Local wind measurements are available in real time at a single location in the Gulf at the ENEA station (Bordone and Lisca 2009), and they show a certain degree of correlation with large-scale southern winds that are less blocked by the surrounding mountains. The local winds during the period June 18–22 are shown in Fig. 3c as stick diagrams (i.e., using the oceanographic conven-

tion indicating the direction of the velocity vector). The wind appears to be mostly directed toward the north–northwest during June 18, in keeping with the large-scale Scirocco pattern (Fig. 3a), but a significant variability can be observed that further intensifies in the following days when also the large-scale winds are more variable. Note in particular a daily fluctuation, with the wind blowing mostly toward the south (i.e., from the Gulf and toward the sea) during the night, and mostly toward the north (i.e., toward the Gulf and from the sea) during the day. This tendency that is observed during the whole period of the experiment especially when the wind is weak is indicative of the presence of land and sea breezes, as it can be expected given the location and the season.

Another set of important local mechanisms influencing the circulation arise due to geometrical effects. The first is the dam that separates the harbor from the rest of the Gulf (Fig. 1). Freshwater flows from several sources inside the harbor and the shallow depth of approximately 10-m act to produce a warmer and fresher water inside the harbor, which drives an estuarine circulation; the water from the harbor tends to exit into the Gulf near the surface via the two lateral openings of the dam (Gasparini et al. 2009). The water in the harbor is replenished by the freshwater sources as well as by the inflow near the bottom through the dam lateral openings. Overall, this implies upwelling rates on the order of $6.5 \times 10^{-6} \text{ m s}^{-1}$ and a residence time of about 5 days inside the harbor (Gasparini et al. 2009). The estuarine-like exchange flow between the harbor and the rest of the Gulf leads to a strongly stratified flow, which responds accordingly to local wind forcing, namely a cyclonic circulation of the surface layer corresponds to an anticyclonic circulation of the deep layer. Finally, the depth of the domain changes gradually with distance from the harbor, reaching 25 m near the Gulf entrance and increasing rapidly toward the open Ligurian Sea. This tends to reduce the effect of the exterior flows on the circulation in the Gulf.

To summarize, the circulation in the Gulf of La Spezia is subject to forcing by large-scale circulation which is modulated by the large-scale wind, as well as by local wind and estuarine circulation. As shown below and in Gasparini et al. (2009) and Molcard et al. (2009), the flow patterns exhibit complex spatial and temporal structures that do not seem to lend themselves to a simple description and pose significant challenges for modeling. As such, the circulation in the Gulf is an ideal example to test whether an approach based on LCS would provide an insight into the observed drifter motion.

The observations include measurements of surface currents using a VHF WERA radar (WERA; Gurgel et al. 1999; Essen et al. 2000) and surface drifters. The data sets from the VHF radar and the drifters have been analyzed and compared in a previous paper (Molcard et al. 2009), where a good agreement in terms of velocity and transport was found. In the following, we briefly review the main characteristics of the two data sets, and the reader is referred to Molcard et al. (2009) for further details.

2.2 The VHF WERA radar data

A dual station of VHF WERA was deployed along the Gulf coast, with the stations situated 7 km apart. The two stations, indicated as ENEA and ROCCHETTA in Fig. 1, had altitudes of 40 and 350 m, respectively. The radar was operated on a 500-kHz-wide bandwidth, covering the radio spectrum from 45 MHz (wavelength of 6.63 m) to 45.5 MHz. At these transmission frequencies, the velocities measured by the radar represent the current at the effective depth of approximately 25 cm (depending on the vertical profile, Steward and Joy 1974). A direction finding (DF or goniometric) method was preferred to the classical beam forming method to compute the radial velocities, in order to improve the azimuth resolution (Broche et al. 2004; Barbin et al. 2006). The typical effective range of the two stations depends on many parameters such as transmit power, altitude of the stations, radioelectrical environment, and geographical and atmospheric conditions, and it is expected to be of the order of 10 km for the present application. A posteriori analysis of the quality of the data indicates that the area in Fig. 1, with range of approximately 7 km, provides radar measurements of good geophysical quality. Maps of radial current components were combined to obtain the vector velocity field on a rectangular grid with resolution of 250 m. The integration time was 7 min twice per hour per radar, the two sites acquiring with a phase shift of 10 min. Current maps of surface total velocity vectors were provided every half hour merging the two radial diphas maps, representing the average state of the ocean during the total 17 min of acquisition.

2.3 The drifter data

The drifters used in the experiment are similar to the ones used in the Coastal Dynamics Experiment (CODE) (Davis 1985; Poulain 1999), but they differ in terms of electronics and antennas for positioning and data telemetry. The drifters were fitted with a small

waterproof container on top of the vertical tubular haul and with a PVC tube protruding over the sea surface to host, respectively, the electronics and antennas of the GPS receiver and the GSM cellular modem. GPS positions were saved every 5–10 min on the internal memory and then sent as SMS messages via GSM to several cellular phones and to a dedicated computer every 15 min. After editing to remove spikes and offsets, the drifter data were interpolated at common times with uniform intervals of 5 min using a cubic spline method. The zonal and meridional components of velocity were estimated by finite differencing the interpolated positions (central differences). The interpolated positions were subsequently low-pass filtered using a Hamming window over an interval of 30 min. These filtered time series were used to compute low-pass filtered velocity series. Relative flow measurements were also performed using one drifter equipped with Nortek Aquadopp acoustic current meter, and they confirmed that the CODE-type drifters used in the experiment followed the surface currents (at a depth of 30 cm) to within 2 cm s^{-1} , in the relatively calm conditions prevailing off La Spezia in June 2007.

While the WERA radar was operated continuously during the period of the experiment, the drifters were launched in four clusters. The first and second clusters consisted of five and six drifters, respectively. These clusters were launched 2 days apart, on June 18 and 20, at the same location (Fig. 1) and were recovered after 14 to 16 and 6 to 24 h of drift, respectively. The third and fourth clusters were launched on June 22 but at two different locations. In these clusters, only two drifters per cluster provided data for a period of 10 to 16 h. Here, we employ trajectories from the first and second clusters since they are more complete, in terms of number of drifters and drift duration. Sampling resolutions of data sources are listed in Table 1.

Table 1 Sampling resolutions of data available in this study

Data source	Spatial resolution (m)	Temporal resolution (min)
VHF radar	250	30
CODE drifters	–	30
Synthetic drifters	–	15
NCOM (finest mesh)	600	180

CODE drifter sampling is continuous in time but available at discrete time intervals in data form. Synthetic drifters are advected using VHF radar-derived velocity fields. NCOM output is not used for Lagrangian analysis due to the inadequate resolution in the Gulf

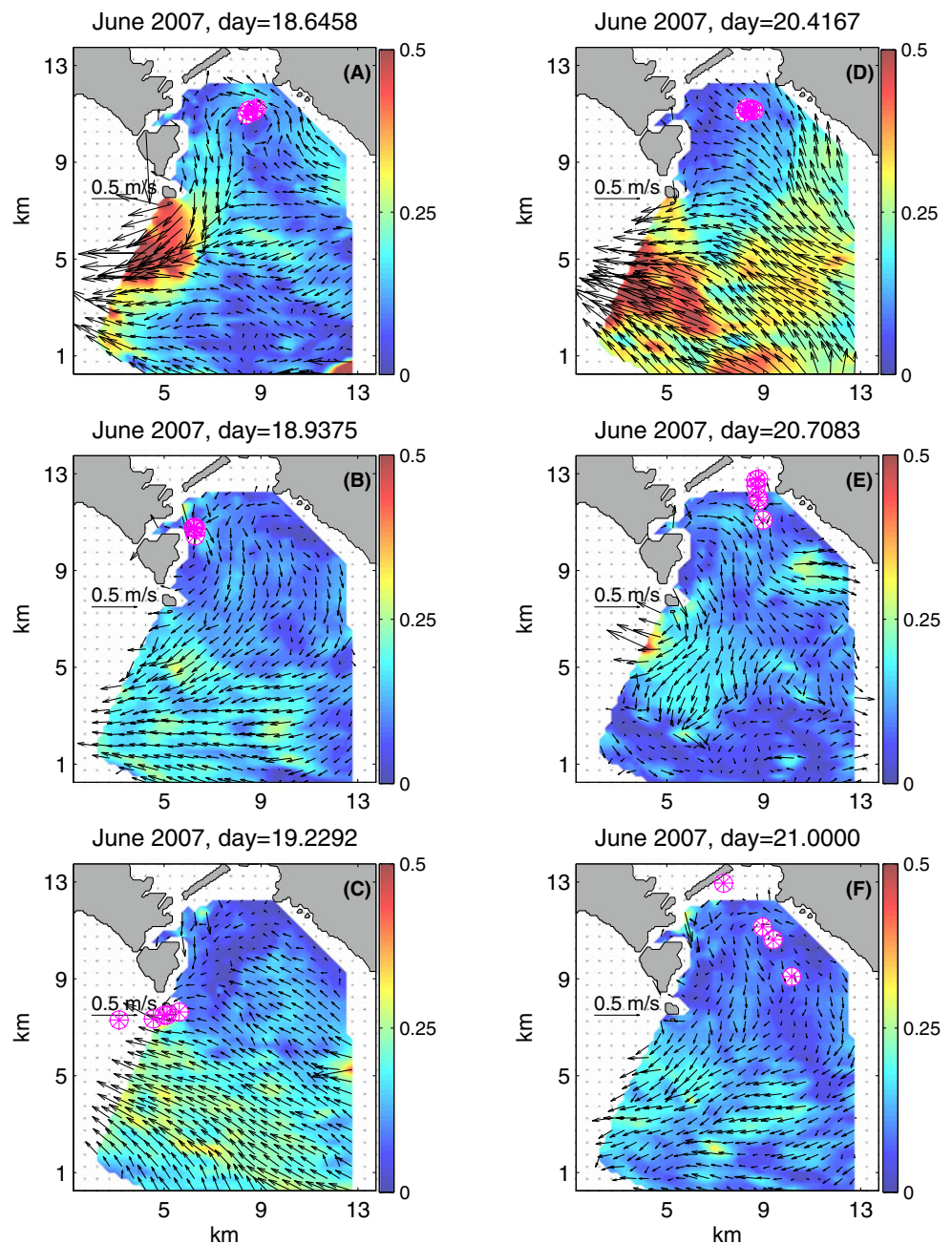
3 Results

3.1 Description and preliminary analysis

The deployment of the drifters in clusters 1 and 2 took place at the center of the Gulf between Fiascherino and Palmaria islands (Fig. 1) and in the shape of a cross with 125 m long legs extending along the north, east, south, and west directions. We recall that the two launches occurred during significantly different meteorological conditions. The first launch, on June 18, occurred during a strong Scirocco episode (Fig. 3a),

when the Ligurian boundary current was strong and close to the coast (Fig. 2a), thereby influencing the local Gulf circulation. The second launch on June 20, instead, corresponds to a period of weaker and more variable winds (Fig. 3b) with a less organized boundary current (Fig. 2b). A total of six drifters were launched in cluster 1 on 18 June 2007 (Fig. 4a). Over the next 14 h, these drifters remained closely clustered and exited the Gulf south of the Palmaria island (Fig. 4a–c; one of them went into the strait near the smaller Tino island just to the south of the Palmaria island). These drifters were advected with the cyclonic circulation in the Gulf that

Fig. 4 Locations of the drifters in cluster 1 at **a** time = 18.65 days in June 2007 (launch time), **b** time = 18.94 days (7 h later), and **c** time = 19.23 days (14 h later) and in cluster 2 at **d** time = 20.42 days (launch time), **e** time = 20.71 days (7 h later), and **f** time = 21.00 days (14 h later). The velocity vectors and speed contours (in meters per second) are superimposed

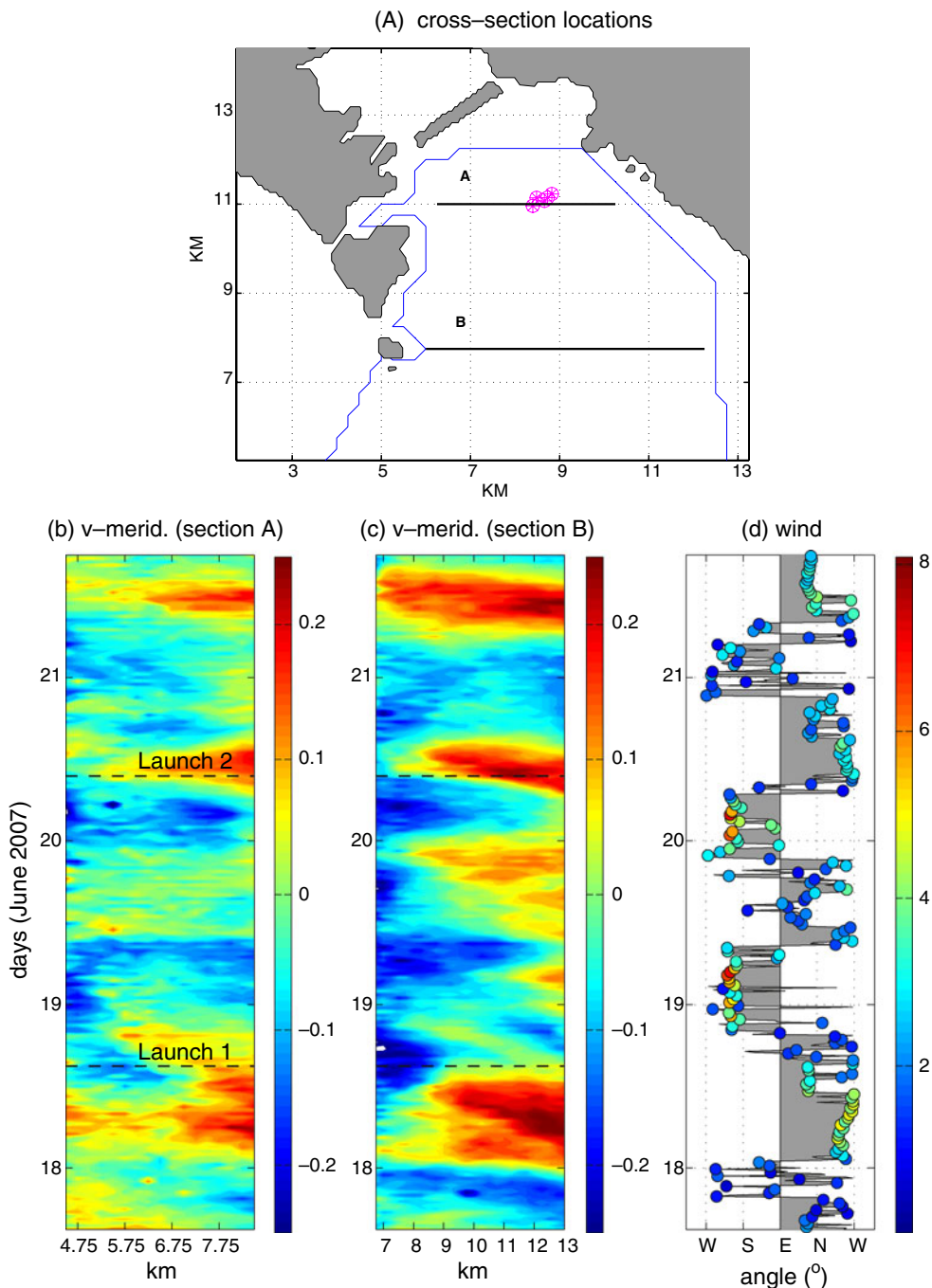


seems to be reinforced by the surface outflow from the harbor along the western gap of the dam, consistent with what is documented by Gasparini et al. (2009). The cyclonic circulation in the northern part of the Gulf is quite persistent during this period, and as such, the Eulerian framework provides a good insight into the drifter motion.

The situation is significantly different for cluster 2 deployed at approximately the same location 2 days later. As an inspection of Fig. 4d–f reveals, the velocity

field is highly variable during the 14 h following the launch. The drifters in this cluster initially move northward together but then start dispersing significantly; two of the five drifters in this cluster remain near the dam (one almost enters the harbor through the eastern gap), while the other three reverse direction and move toward the southeast. In this case, the temporal variability of the velocity fields acting on the drifters is complex enough to prevent a direct conclusion on the basis of several snapshots of the Eulerian field. The

Fig. 5 **a** Geographical locations of sections *A* and *B*. **b** Hovmoeller diagrams of velocity $v(x, t)$ (in meters per second) normal to sections *A* and *c* (positive values are pointed northward) during the launch periods of clusters 1 and 2. **d** Temporal evolution of the wind direction angle (90° indicates northward direction) and magnitude (in colors) from the local Enea station during the same period. The color bars indicate speed in meters per second



branching and rapid spreading of the cluster indicate the possible presence of a (transient) hyperbolic trajectory and motion along outflowing manifolds in this case. As such, the analysis of the motion of this cluster may benefit from the computation of LCS.

In order to get a better sense of the time variability of the velocity fields, Hovmoeller diagrams are plotted of the velocity normal to two zonal sections, denoted **A** and **B**, intersecting the pathways of the drifters (Fig. 5a–c). In general, the trends at these two sections seem to correlate well. Northward motion (indicated by positive values of the meridional velocity) can be clearly seen along the eastern segments of these sections, while southward motion (negative values) prevails along the western segments, consistent with the cyclonic circulation reported in Gasparini et al. (2009). These plots also reveal a significant degree of temporal variability at various frequencies. The direction of the circulation seems to occasionally reverse, or sometimes there is a net northward or southward flow spanning the entire sections.

The Hovmoeller diagram of the wind speed angles from the local Enea station (Fig. 5d) is compared to that of meridional surface velocities (Fig. 5b, c). The wind index exhibits a daily signal, probably related to the presence of land and sea breezes as discussed in Section 2.1. As for the currents, a certain degree of correlation with the wind can be noticed. Winds from the north–northeast occurring mostly at night and persisting over half a day tend to generate southward currents, in particular on the western side of the domain, while winds from the south–southeast occurring during the day tend to generate northward velocities on the eastern part of the domain. The circulation variability, though, appears more complex, showing periods of complete reversal and suggesting additional periodicities.

In order to better quantify the time variability evident in these plots, frequency power spectrum of $v(x = 8.25 \text{ km}, t)$ at section **B** during the period of $17.625 \leq t \leq 21.625$ days is computed (Fig. 6). The frequency spectrum shows peaks located at many frequencies, with most of the power concentrated at approximately diurnal and semidiurnal frequencies, with corresponding periods of 19.9 and 12.4 h, respectively. The 19.9-h period indicates inertial motion, likely to be related to wind fluctuations, while the 12.4-h period might be related to the presence of tides, even though their energy is significantly smaller than for inertial, as it is expected in the Ligurian Sea.

It is of interest to explore the spatial structure of the VHF radar-derived surface flow field by computing the wavenumber power spectrum of kinetic energy.

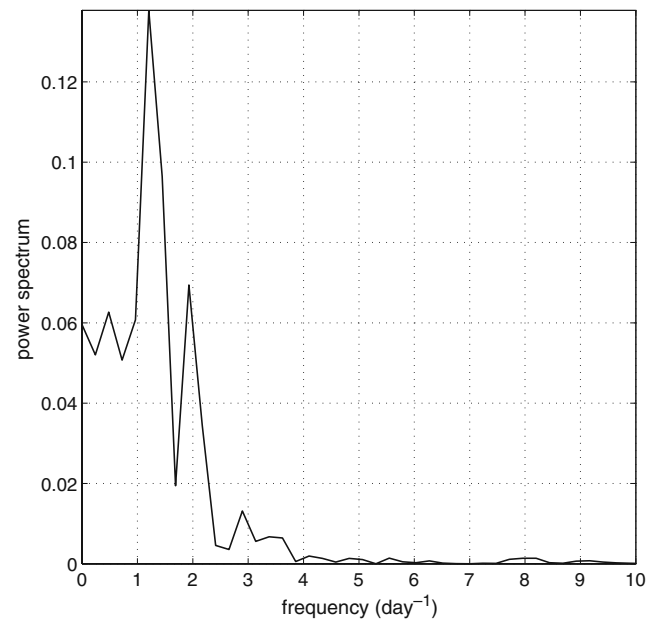


Fig. 6 Frequency power spectrum of the velocity component normal to section **B** during the period of $17.625 \leq t \leq 21.625$ days of June 2007

Bennett (1984) classified the submesoscale tracer dispersion as a function of the kinetic energy spectrum, in that if the slope of the spectrum is steeper than -3 , then there is no significant energy at scales below the main mesoscale turbulent features, and the tracer transport is controlled by persistent, energetic mesoscale turbulent features (so-called nonlocal dynamical regime). If on the other hand the spectral slope is shallower, then this is an indication of significant energy at small scales (so-called local regime). The radius of deformation here can be estimated from $R_d \approx \sqrt{g'h/2}/f$ by assuming a two layer flow, where $g' \approx 10^{-2} \text{ m}^2 \text{ s}^{-2}$ and $h \approx 10 \text{ m}$ from Fig. 7 of Gasparini et al. (2009) and $f \approx 10^{-4} \text{ s}^{-1}$. Thus, we get an estimate for the mesoscales as $R_d \approx 2.2 \text{ km}$, which is comparable to the width of the domain and provides a wavenumber range of only a decade with respect to the VHF radar resolution of 250 m. The Rossby number can be estimated from $Ro = U/(f R_d)$. Using $U \approx 0.2 \text{ m s}^{-1}$, one gets $Ro \approx 1$, which implies that submesoscale processes can be important (Thomas et al. 2008).

The wavenumber power spectrum is computed on the basis of ten meridional sections along the 2.5-km-wide strip in the middle of the observational domain and by taking the spatial average of the spectrum in order to reveal the scales of motions that carry significant energy. In addition, this is done for four different snapshots during the experiment in order to investigate how the spectrum changes in time. Figure 7

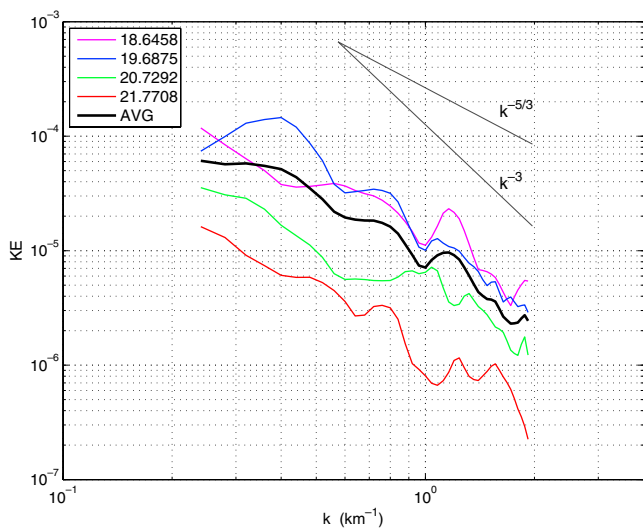


Fig. 7 Wavenumber power spectrum of kinetic energy for meridional sections in the observational domain at four different times, $t = 18.6458$ (magenta), $t = 19.6875$ (blue), $t = 20.7292$ (green), $t = 21.7708$ (red) of June 2007, and their average (black)

shows the spectra within a wavelength range of 5 and 0.5 km (half the domain size and double the grid size via the Nyquist rule). Spectra at individual times show various peaks at various wave lengths, straddling $k^{-1} \approx 1$ km. The spectra show a great degree of sensitivity to time. While the broadband slope of the spectrum appears to be shallower than -3 , the peaks migrate between different wavenumbers at different times. For instance, the power KE peak at $k \approx 1.2 \text{ km}^{-1}$ at $t = 18.6458$ days appears to induce both upward and downward traveling peaks at later times, while the overall energy levels

are reducing simultaneously. This indicates that the spectrum is not fully developed (in equilibrium) but dominated by transient events that appear to revolve around features whose size is comparable to R_d .

The sensitivity of the Lagrangian motion to launch locations and times is shown by releasing synthetic drifters in the VHF radar-derived velocity field along section **A** during three different periods. Synthetic drifters launched simultaneously with cluster 1 show almost no dependence on location; all seem to follow the cyclonic pathway described above (Fig. 8a). On the other hand, synthetic trajectories launched along section **A** with cluster 2 are far more complex, most indicating an anticyclonic transport while those near the coast exhibit very small velocities (Fig. 8c). Finally, synthetic drifters are also released at an intermediate time, which exit the Gulf along a different, jet-like path (Fig. 8b).

In order to gain a better insight in the overall picture, 3,700 synthetic particles are launched on a regular grid, and their positions after 6 h are depicted in Fig. 9 for four realizations starting at different times. In all cases, large-scale straining and control exerted by the ambient flow field (Ligurian current) is quite striking. Particles tend to exit the observational domain along a narrow corridor at the right/western boundary. There are also indications of convergence and divergence zones.

Overall, Figs. 4–9 appear to indicate that this flow is mostly characterized by temporal variability of broad (on the order of the radius of deformation) flows in this Gulf, which appear to be controlled mainly by changes in the larger-scale Ligurian current and modulated by

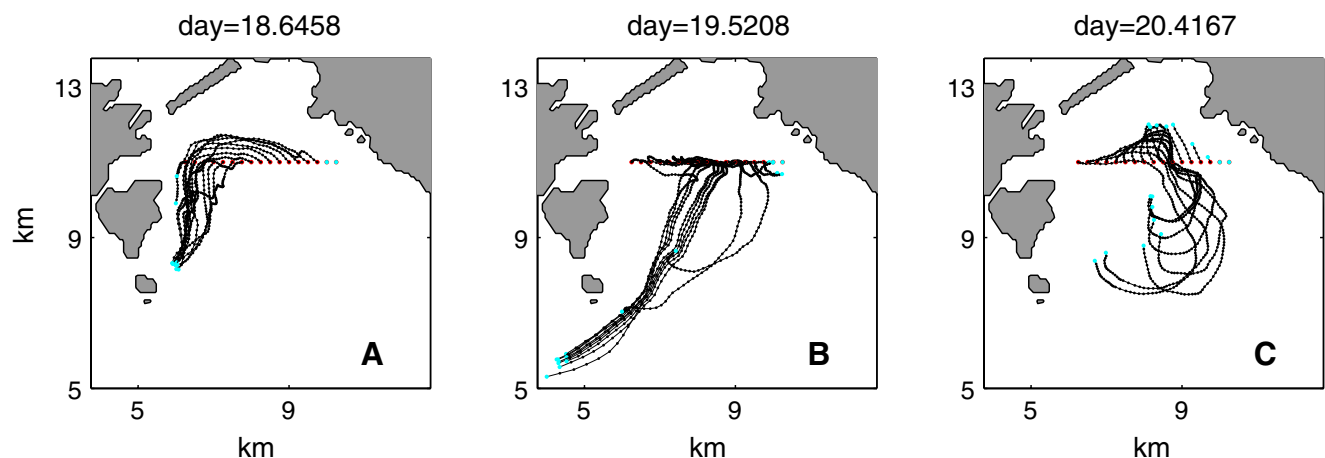
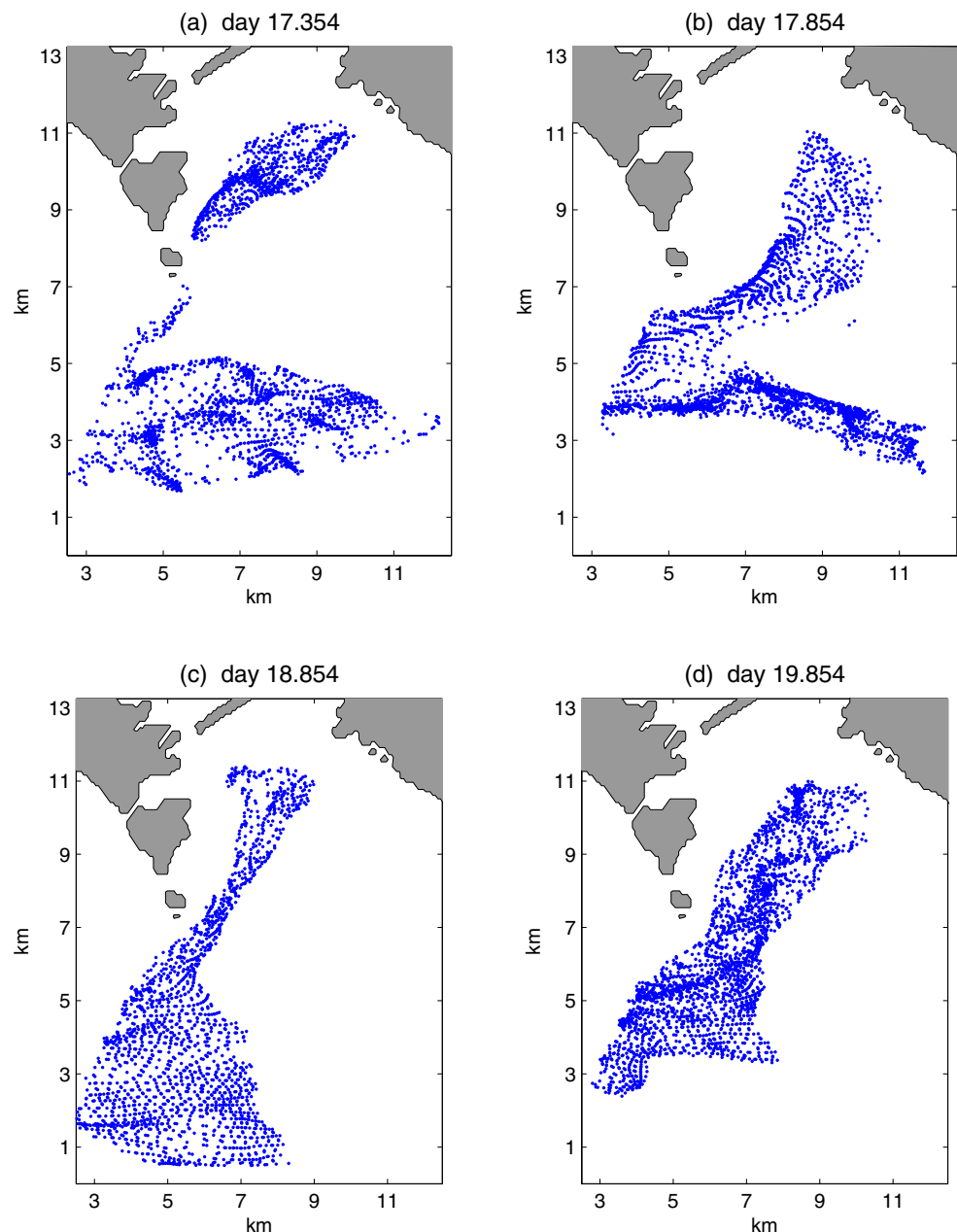


Fig. 8 One-day-long trajectories of synthetic drifters advected with the VHF radar-derived velocity fields after being launched at section **A** at three different times, **a** $t \approx 18.6$ days (same as

cluster 1), **b** $t \approx 19.5$ days **c** $t \approx 20.4$ days (same as cluster 2) of June 2007. Red color marks the initial locations and blue color the final locations

Fig. 9 Locations of particles 6 h after being launched on a regular grid in the domain for four releases at different times during the experiment



the local wind forcing. The width of the Gulf is comparable to the radius of deformation, which could be a factor in that long-lasting, isolated coherent structures are not observed. The turbulent breakdown of the existing flows via eddies and filaments is not evident from this data set either; these could be taking place at spatial and temporal scales smaller than the resolution of the VHF radar. We conclude that the circulation in the Gulf of La Spezia is complex enough not to readily fit in the regime of more conventional, quasigeostrophic flows, which are characterized by slowly varying and clearly defined geometric features such as jets and ed-

dies. In other words, the flows in the Gulf of La Spezia appear to have a character of forced (both through the boundaries and locally), geometrically constrained turbulence, rather than free turbulence in the open ocean. As such, measurements in the Gulf of La Spezia appear to provide an interesting testbed for the validity of LCS to characterize Lagrangian transport.

3.2 Drifter motion in comparison to the FSLE

Given the importance of temporal variability in these flows, it is of interest to explore whether the LCS

can provide a complementary insight into the observed drifter motion. The LCS are estimated from the FSLE defined as

$$\lambda(\delta_0, \alpha) = \frac{\log(\alpha)}{\tau(\delta_0, \alpha)}, \quad (2)$$

where τ is the time required for a particle pair to separate from an initial distance δ_0 to a final distance $\alpha \times \delta_0$. The FSLE fields highlight zones of particle convergence and divergence due to (at least) three effects: (a) in-flowing and out-flowing manifolds created by the geometry and motion of coherent structures like jets and eddies, (b) shear dispersion, and (c) convergence zones due to 3-D effects.

The FSLE is computed by launching synthetic drifters in the VHF radar-derived velocity fields in a cross configuration corresponding to four particle pairs initially separated by 56.25 m on a regular grid, and a total of 24,500 particles are used. The ensemble of particles is advected both forward and backward in time for 12 h, with a time step of $\Delta t = 15$ min, which is half the radar temporal sampling period needed for the fourth order Runge–Kutta particle advection method. Both advectations are reinitialized every 30 min. The FSLE fields are computed in 2-D given the nature of the observations. It is important to point out that CODE drifters are designed to stay at the surface so that the comparison of this independent measurement is consistent with the use of a 2-D velocity field.

The choice of α is based on the need to both visualize adequate details of the FSLE extrema and the constraints of a spatially limited domain where the particle pairs at the edge can exit before reaching the required distance $\alpha\delta_0$. The choice of an optimal value for α when computing the ensemble FSLE as a function of delta has been discussed initially by Lacorata et al. (2001). If α is too large (usually $\alpha > 2$ depending on the type of flow and time discretization of the model), then relative dispersion from small coherent features is not well captured. If on the other hand, α is too close to 1, then aliasing problems related to the time step of particle advection may yield a spurious FSLE plateau at small scales (Fig. 2b in Haza et al. 2008). The optimum α is usually the smallest value for which λ_{\max} is not affected by aliasing. Here, the FSLE computed with higher values of α (1.4, 2.0) have given the same results, which is an indication that $\alpha=1.2$ is in the optimal range. Larger values of α , such as $\alpha > 2$, are usually picked to compute spatially local FSLEs in order to map the Lagrangian coherent structures. For a limited duration of the experiment, a small α will give nonzero FSLE values all over the domain and will overcrowd the

map, while a large α will give nonzero values only in a few spots of very high dispersion and the map will be mostly blank. If the flow is highly variable in time, it is a better strategy to reduce α . In this case, we are also constrained by the short residence times of the particles. A good trade-off appears to be achieved with $\alpha = 7$ for the FSLE maps that follow.

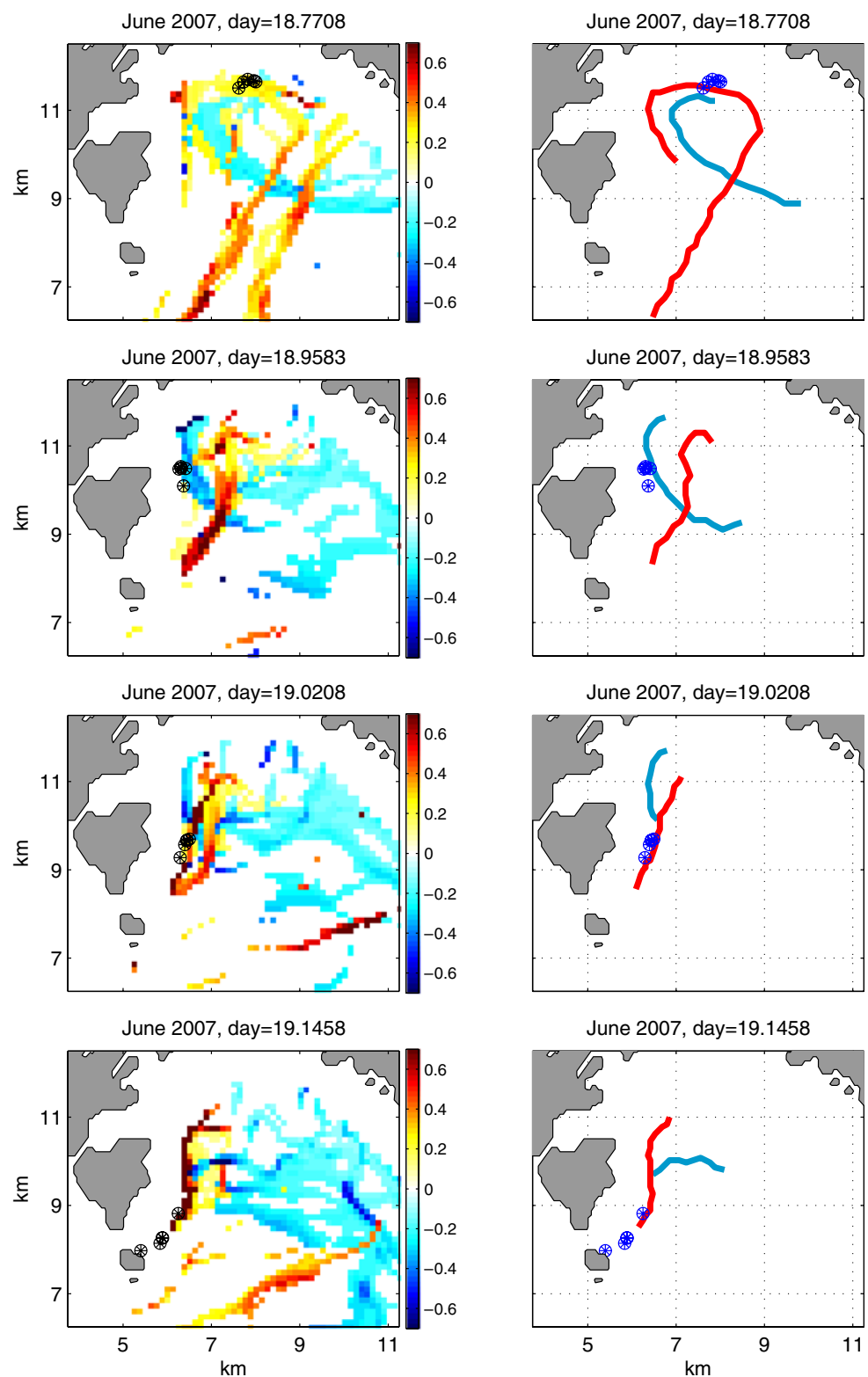
The FSLE extrema are displayed as cyan and blue areas for highest dispersion values and as yellow and red areas for highest concentrations (Figs. 10 and 11). An animation of the FSLE ridges superimposed with the motion of the two drifter clusters can be downloaded from: http://www.rsmas.miami.edu/personal/ahaza/radar/LaSpezia_fsle_clusters.gif. The FSLE ridges (where the FSLE are extremum) tend to appear as bands entangled like a spider web, evolving in space and time with the flow, and their motion is consistent with the inertial oscillations visible when the main currents south of the domain slacken, as well as with the entrainment of these same currents, and the predominant cyclonic circulation in the Gulf. This behavior is highlighted by selecting the main FSLE ridges and digitizing it for several time frames in conjunction with the drifter positions (Figs. 10 and 11, right columns).

While the motion of cluster 1 appears fairly easy to explain on the basis of the persistent cyclonic flow in Fig. 4 (left column), the computation of the FSLE reveal two opposite extrema (Fig. 10). As shown in Fig. 10 (left column), the curved yellow (high concentration) ridge controls the motion of the drifters until the blue ridge intersects their path, at which point they begin to follow its edge for a while. The drifters later exit the domain on the edge of another ridge of high concentration.

In the case of cluster 2, the launch location appears to have coincided with the location of what seems to be a hyperbolic trajectory, characterized by the intersection of positive and negative FSLE ridges (Fig. 11 left column). Three drifters have been released on each side of the in-flowing branch (or branch of maximum dispersion) and all drifters are evolving along the out-flowing branch (yellow band isolated in the left column of Fig. 11). It is clear that the three drifters disperse pretty fast and move along the edge of the yellow ridge, while the ridge itself is evolving both in space and in shape. While covering a maximum distance of 3.8 km, the drifters stay within a maximum distance of 0.3 km from the ridge, an order of magnitude shorter (right column in Fig. 11).

The motion of both drifter clusters superimposed on the FSLE fields show that the drifter motion is consistent with the spatial and temporal evolution of

Fig. 10 *Left panel* Spatial distribution of FSLEs (in per day) computed forward in time (positive) and backward in time (negative) with the observed drifters in cluster 1. *Right panel* The main FSLE ridges that appear to be controlling the drifter trajectories

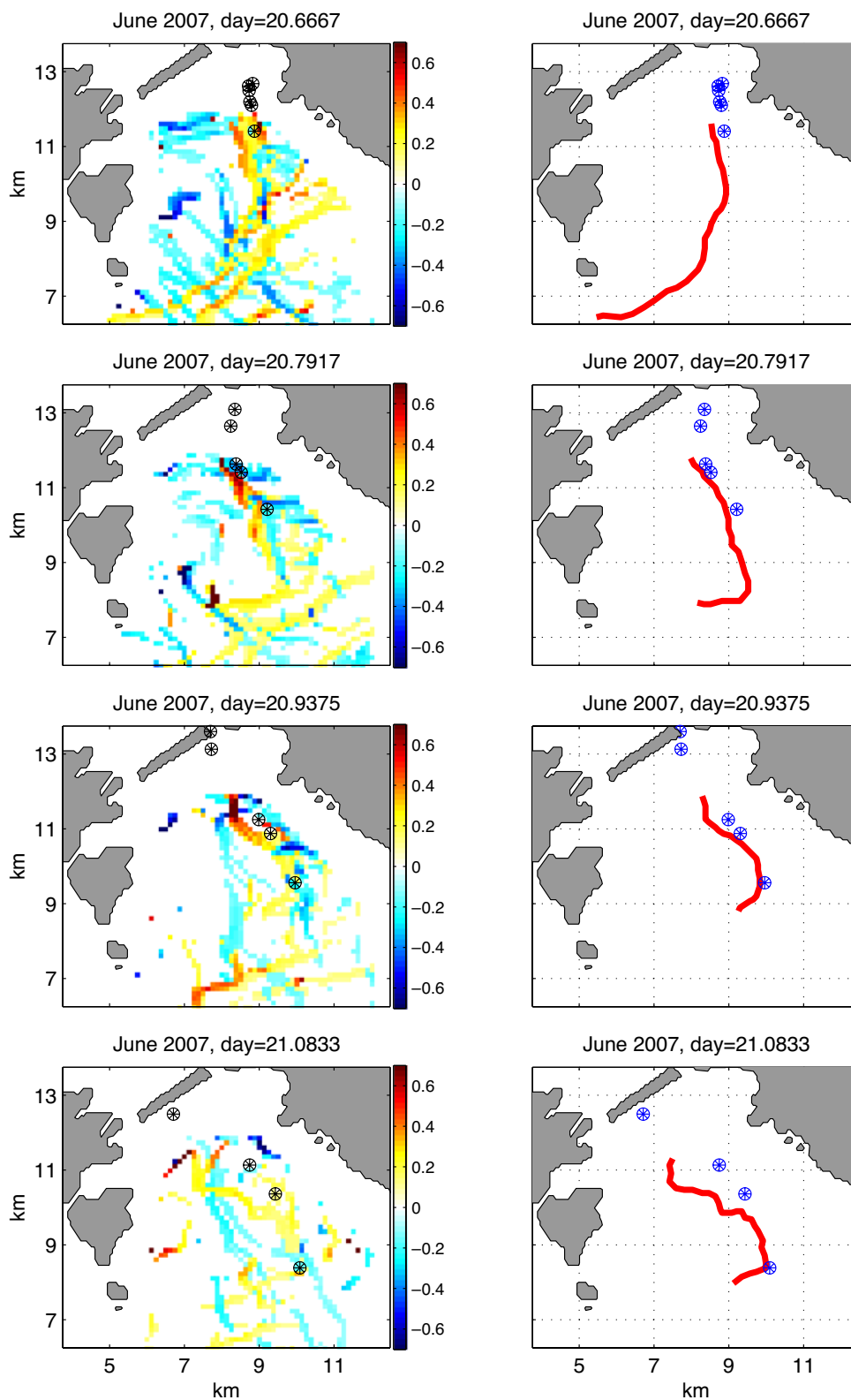


the FSLE fields. Additionally, the drifters appear to follow, yet not cross the FSLE ridges, thus confirming the correspondence of the FSLE ridges with the natural transport barriers of the flow.

3.3 Relative dispersion

Another useful quantity is the spatial average of the FSLE maps, which provides a single value for the

Fig. 11 Same as Fig. 9, but for cluster 2



separation time of pairs initially launched at specific scales for the entire domain. Since relative dispersion is inherently connected to lateral mixing, $\lambda(\delta)$ is of

great interest. In particular, $\lambda(\delta)$ is a powerful way of exploring the relationship between the temporal and spatial scales affecting tracer dispersion in a sin-

gle simple plot. Of particular interest is what happens at scales below the mesoscale coherent structures. If the nonlocal dynamical regime dominates (dispersion at submesoscales is controlled by persistent, energetic mesoscale turbulent features), then one would expect the FSLE to be scale independent and assume a constant value at the submesoscale part of the plot (so-called exponential regime). If, on the other hand, the local dispersion regime holds (relative dispersion is dictated by the small and rapidly evolving scales), then one does not expect to see an exponential regime in $\lambda(\delta)$ but rather the relative dispersion to be scale dependent, namely to increase as the spatial scales get smaller.

An accurate investigation of the local and nonlocal dispersion regimes proved to be challenging for oceanic flows not only because of the lack of an adequate number of simultaneously deployed drifters but also because ocean models typically do not resolve all scales of motion, in particular the submesoscale dynamics. Some of the relevant studies employing observational data is the one by LaCasce and Bower (2000) in the Gulf Stream region, which was inconclusive due to low number of drifter pairs. LaCasce and Ohlmann (2003) targeted the Gulf of Mexico, which was far more rich with 140 drifter pairs, and found an exponential regime for scales less than 1 km. In contrast, Lumpkin and Ellipot (2010) could not identify an exponential regime down to 300–500 m from a data set consisting of 55 closely launched drifters near the Gulf Stream. Since these observations were taken under substantial wind forcing, they indicate the presence of significant submesoscale motion influencing particle spreading. The study by Haza et al. (2008) using NCOM with 1 km resolution indicated that the exponential regime in $\lambda(\delta)$ can be quite sensitive to inhomogeneities in the flow field and the sampling method in that the shear dispersion induced by the Western Adriatic Current and chance-pair sampling tends to influence the exponential regime. A fairly comprehensive follow-up study was then undertaken by Poje et al. (2010) using a hierarchy of models, ranging from 2-D turbulence simulations, progressing to idealized simulations of a buoyant coastal jet with ROMS, and finally to realistic HYCOM simulations of the Gulf Stream. The main finding of this study is that, in each case, relative dispersion at large time and space scales is found to be controlled by energetic mesoscale features of the flow which are relatively insensitive to the resolution of finer scale motions, while the relative dispersion at smaller scales is characterized by an exponential regime. Nevertheless, observational data for the submesoscale range remains rare. As such, it is of great interest to explore

this issue to reveal the multiscale interactions at various places in the ocean.

In order to compute $\lambda(\delta)$ from the VHF radar-derived velocity fields, a total of 3,700 particles arranged on a cross configuration on the radar grid were launched and advected forward for 12 h. An additional problem that we encounter here with respect to previous studies in a semi-enclosed Adriatic Sea (Haza et al. 2008) and realistic North Atlantic modeling (Poje et al. 2010) is that the Gulf of La Spezia domain is quite small with open boundaries. As a result, the amount of time spent by the particles inside the domain observed by the radar is far less than the total duration of the observations. In order to fully utilize the observations, the synthetic particle launches are re-initialized every 12 h for a total of ten times during the period of $17.625 \leq t \leq 22.625$ days. After June 23, complex nonlinear effects associated with the wind created a swell formation which induced a modulation of the short waves. This is a well-known shallow water effect (Barrick and Lipa 1986), which is translated in the Doppler spectrum as a “trident” shape that is very difficult to read and follow in time. While the analysis of this effect and the surface current estimation is still an on-going work, here we decided to limit the relative dispersion analysis to a smaller dataset on which we were confident.

Two complementary launch strategies are adopted here to compute $\lambda(\delta)$. First, the four initial pairs are centered on the radar grid point, with an initial distance $\delta_0 = 0.45 \times 0.250 \text{ m} = 112.5 \text{ m}$. In this case, only $\lambda(\delta = 112.5 \text{ m})$ is estimated from original pairs, while $\lambda(\delta)$ for $\delta > 112.5 \text{ m}$ is computed on the basis of chance pairs. Chance-pair sampling may sometimes introduce a bias for sampling preferentially the fast-dispersing pairs, as discussed in Haza et al. (2008). Therefore, additional launches were conducted with original-pair configurations of $\delta_0 = 250 \text{ m}$, $\delta_0 = 500 \text{ m}$, and $\delta_0 = 1,000 \text{ m}$. Then the separation of these tagged pairs are tracked between δ and $\alpha\delta$, where $\alpha = 1.2$.

The resulting λ curves obtained for δ in the range of 0.1125 to about 1–2 km (Fig. 12) show some variability for the ten different realizations, but overall, all of them indicate fairly constant values; their average varies between $\lambda \approx 5 \text{ day}^{-1}$ and $\lambda \approx 7 \text{ day}^{-1}$ from chance pairs and $\lambda \approx 5 \text{ day}^{-1}$ and $\lambda \approx 4 \text{ day}^{-1}$ from original pairs. There is some indication that the FSLE is decreasing for scales larger than 1 km, but due to the small area of radar coverage, the behavior of the FSLE scales equal to and larger than the radius of deformation cannot be quantified. The approximately constant $\lambda(\delta)$ identifies an exponential regime, indicating that the relative dispersion at these scales is nonlocal, namely mostly controlled by dynamics of the large-scale straining field. In

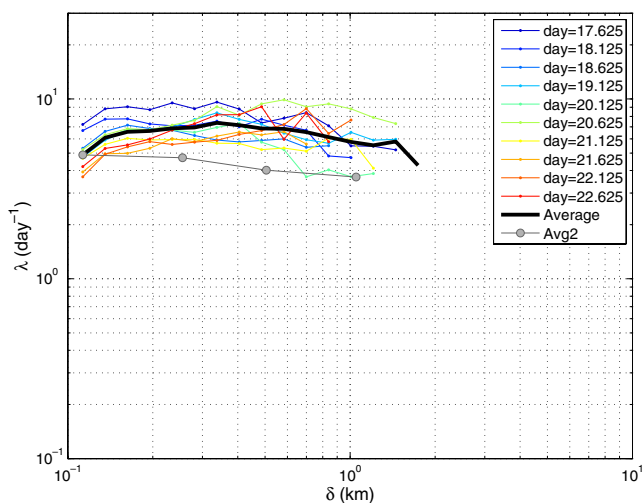


Fig. 12 Spatial dependence of FSLE, $\lambda(\delta)$, from Lagrangian particle releases at ten subsequent samplings during the period of $17.625 \leq t \leq 22.625$ days (colored curves) and their average (thick solid curve). The gray thick curve shows the average FSLE resulting from additional launches with original pair separations of 250, 500, and 1,000 m

other words, any significant control by rapidly evolving, small-scale turbulent structures on relative dispersion appears to be precluded on the basis of Fig. 12.

In order to confirm this conclusion, relative dispersion is computed using also the more classical mean-square particle pair separation (Richardson 2001),

$$D^2(t) = \langle |\mathbf{x}^{(1)}(t) - \mathbf{x}^{(2)}(t)|^2 \rangle, \tag{3}$$

where the average is over all pairs of particles in the cluster. The results of D^2 are shown for $15 \text{ min} \leq t \leq 12 \text{ h}$ in Fig. 13. A log–log plot (Fig. 13a) does not seem to reveal a clear power law fitting well to diffusive $D^2 \sim t$, ballistic $D^2 \sim t^2$, and Richardson $D^2 \sim t^3$ regimes, while a semilog plot (Fig. 13b) shows approximately constant slopes characteristic of an exponential regime for the first 6 h. By assuming $D^2(t) = D^2(0) \exp(2\lambda_0 t)$ and substituting values of $D^2(0) = (0.1125 \text{ km})^2$, $D^2(t = 6.5 \text{ h}) \approx 0.05 \text{ km}^2$ for the averaged curve, one gets $\lambda_0 \approx 2.5 \text{ day}^{-1}$, which is close to the FSLE values in Fig. 12.

The magnitude of the relative dispersion from VHF radar observations in the Gulf of La Spezia is compared to those obtained by Haza et al. (2008) from NCOM simulations of the Adriatic Sea, as well as those from the recent study by Poje et al. (2010), in which an idealized buoyant coastal current was modeled using ROMS and the Gulf Stream region with a realistic HYCOM simulation (Fig. 14). NCOM simulations show an exponential regime with $\lambda_{\text{max}} \approx 0.6 \text{ days}^{-1}$ for $\delta < 10 \text{ km}$. The result from HYCOM indicate an exponen-

tial regime for scales smaller than 50 km (the radius of deformation for this flow is 35 to 50 km), where the value of the maximum exponent is about $\lambda_{\text{max}} \approx 0.4 \text{ days}^{-1}$. This value is also in agreement with that inferred by LaCasce and Ohlmann (2003) in the Gulf of Mexico with the SCULP data. The smaller-scale ROMS simulation with a radius of deformation of 5 km also indicates an FSLE plateau with a somewhat higher value of $\lambda_{\text{max}} \approx 0.8 \text{ days}^{-1}$. These values are about an order of magnitude lower than those estimated from the present VHF radar observations. While not showing a clear exponential regime, the FSLE curve computed by Lumpkin and Ellipot (2010) on the basis of CLIMODE drifter pairs exceeds the value of $\lambda_{\text{max}} \approx 10 \text{ days}^{-1}$ for $\delta < 3 \text{ km}$, which is somewhat higher than

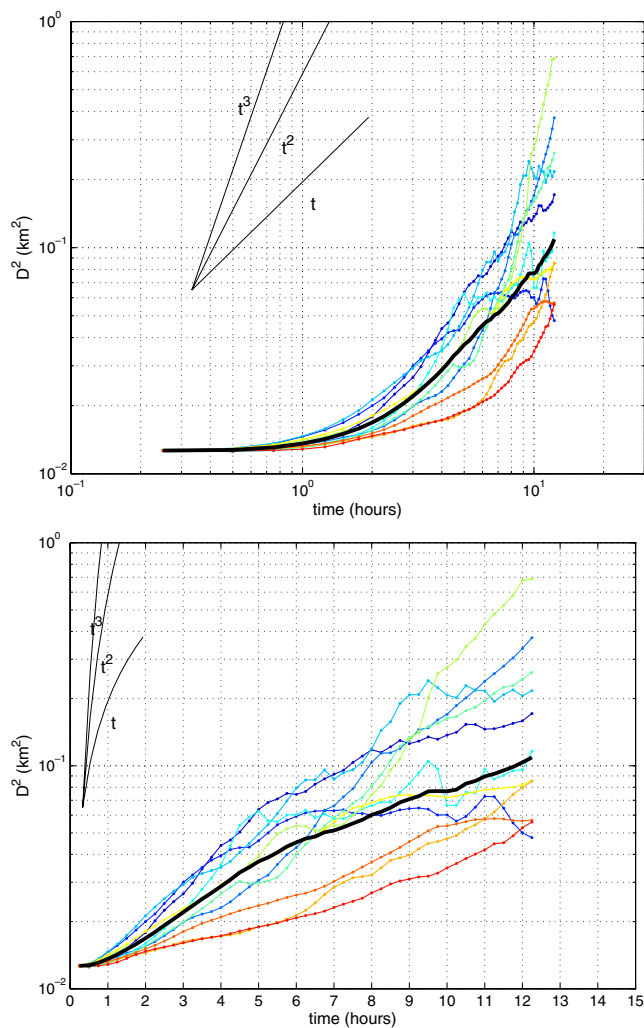


Fig. 13 Relative dispersion $D^2(t)$ as a log–log plot (upper panel) and semilog plot (lower panel). The curves corresponding to diffusive $D^2 \sim t$, ballistic $D^2 \sim t^2$ and Richardson $D^2 \sim t^3$ regimes are marked. Refer to the inset of Fig. 12 for the explanations of the different curves

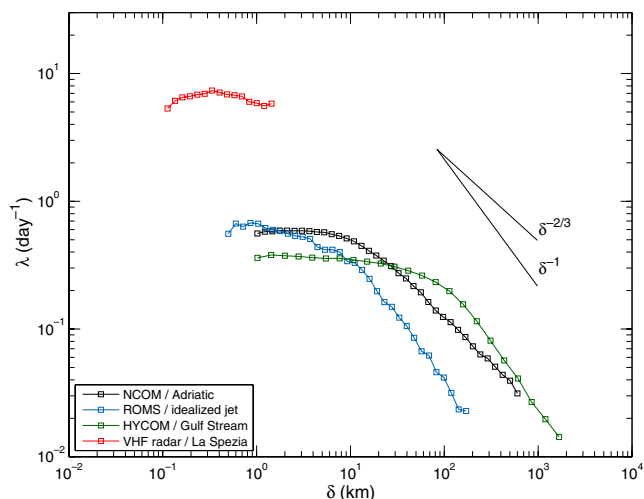


Fig. 14 FSLE curves $\lambda(\delta)$ from the present study, as well as those obtained on the basis of models presented in Poje et al. (2010), namely simulation of a buoyant coastal jet with 0.5 km horizontal resolution ROMS (blue) and the Gulf Stream region with 1/12° HYCOM (green) and 1 km NCOM (black) simulations of the Adriatic Sea circulation studied in Haza et al. (2008). All curves are obtained using original pairs. The slopes corresponding to ballistic $\lambda \sim \delta^{-1}$ and Richardson $\lambda \sim \delta^{-2/3}$ regimes are marked

the λ_{\max} obtained from the VHF radar measurements here (Table 2).

3.4 Scaling of the FSLE with the Okubo–Weiss parameter

A useful Eulerian quantity commonly used to characterize the coherent structures in turbulent flows is the Okubo–Weiss criterion Q (Okubo 1970; Weiss 1991):

$$Q^2 = S^2 - \omega^2 = (\nabla \times \mathbf{U}_H)^2 + 4 \left(\frac{\partial u}{\partial y} \frac{\partial v}{\partial x} - \frac{\partial u}{\partial x} \frac{\partial v}{\partial y} \right), \tag{4}$$

where $S^2 = \left(\frac{\partial u}{\partial x} - \frac{\partial v}{\partial y} \right)^2 + \left(\frac{\partial v}{\partial x} + \frac{\partial u}{\partial y} \right)^2$, is the horizontal strain rate, $\omega = \frac{\partial v}{\partial x} - \frac{\partial u}{\partial y}$ the horizontal vorticity, and $\nabla \cdot \mathbf{U}_H = \frac{\partial u}{\partial x} + \frac{\partial v}{\partial y}$ the horizontal flow divergence.

One of the important results of the study by Poje et al. (2010) was to show that the limiting (maximum) value of the FSLE plateaus well with the resolved Eulerian velocity gradients as given by the average positive Q , denoted $\langle Q^+ \rangle^{1/2}$ here, which distinguishes regions of strain from regions of rotation, thereby quantifying the hyperbolicity in the field:

$$\langle Q^+ \rangle^{1/2} = \sqrt{A^{-1} \int Q dA}, \text{ for } Q > 0, \tag{5}$$

where A is the area of the observational domain. Given the FSLE plateau in Fig. 12, indicating that hyperbolic regions are generated by nonlocal dynamics, it is of interest to investigate whether λ_{\max} scales with $\langle Q^+ \rangle^{1/2}$ for the Gulf of La Spezia as well.

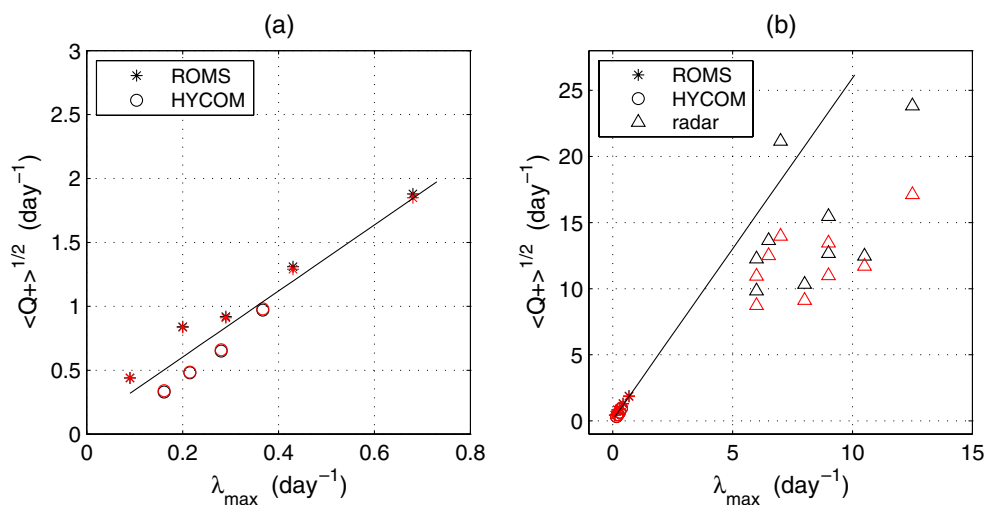
The primary concern here is the potential effect of the horizontal divergence field. Even in the presence of high horizontal divergence, they need to be long lasting in order to exert a significant control on relative dispersion. One particular process that may accomplish this is the Langmuir circulation (Langmuir 1938), which tends to create bands of convergence/divergence zones that are typically 2–300 m apart and some ten times greater in length with vertical velocities reaching as high as 25 cm/s (Weller and Price 1988). Langmuir cells arise from the interaction between the Stokes drift due to surface waves and the vertical shear of the wind-induced currents (Craik and Leibovich 1976). Large eddy simulations of this process revealed very complex patterns (Skylingstad and Denbo 1995). Given the radar resolution of 250 m and lack of adequate wind data and vertical profiles in the Gulf, it seems not feasible to explore the existence of Langmuir cells in detail here. Nevertheless, the impact of the horizontal divergence with respect to that of large-scale straining on the relative dispersion can be quantified based on the radar data.

Figure 15a shows the scaling of λ_{\max} with $\langle Q^+ \rangle^{1/2}$ on the basis of numerical modeling in Poje et al. (2010), with the solid line showing the least-square linear fit to the relationship. In Fig. 15b, λ_{\max} vs $\langle Q^+ \rangle^{1/2}$ from the VHF radar data is included, and it seems that they

Table 2 Comparison of the characteristics of exponential regimes from different studies

Model	Data	Region	λ_{\max} (days ⁻¹)	FSLE plateau	Citation
NCOM	–	Adriatic Sea	0.6	For $\delta < 10$ km	Haza et al. (2008)
ROMS	–	Idealized	0.7	For $\delta < 4$ km	Poje et al. (2010)
HYCOM	–	Gulf Stream	0.4	For $\delta < 50$ km	Poje et al. (2010)
–	SCULP drifters	Gulf of Mexico	0.3	For $\delta < 20$ km	LaCasce and Ohlmann (2003)
–	CLIMODE drifters	Gulf Stream	10	–	Lumpkin and Ellipot (2010)
–	VHF radar	Gulf of La Spezia	4 to 7	For $\delta < 1$ km	This study

Fig. 15 Scatter plots of λ_{\max} vs $\langle Q^+ \rangle^{1/2}$ **a** from simulations in Poje et al. (2010) and **b** with results from Gulf of La Spezia. The red (black) symbols indicate $\langle Q^+ \rangle^{1/2}$ computed without (with) the horizontal divergence term. The linear least-square fit to the data from Poje et al. (2010) is shown by a straight line



cluster generally somewhat below the linear scaling. Nevertheless, this result is a reasonable success given that the linear prediction is based purely on modeling of different types of flows and many sources of errors that can take place in measurements. In order to explore effect of the horizontal divergence, we computed $\langle Q^+ \rangle^{1/2}$ with the $(\nabla \cdot \mathbf{U}_H)^2$ in Eq. 4. Horizontal divergence effects are negligible in ROMS and HYCOM simulations. After all, these are hydrostatic models with 0.5 and 8 km resolutions, respectively, simulating mainly geostrophic turbulence. Nevertheless, we find a change in the scatter plot between λ_{\max} with $\langle Q^+ \rangle^{1/2}$, possibly a slight deterioration of the fit when the horizontal divergence is removed. This implies that horizontal divergence plays some role in relative dispersion, albeit much smaller than that by the large-scale straining field.

4 Summary and conclusions

Surface transport characteristics in the Gulf of La Spezia, which is a small-scale feature along the western Italian coast, are explored using the VHF radar observations collected in the context of POET-LASIE experiment for 2 weeks in the summer of 2007. In addition, an independent data set from two clusters of CODE type surface drifters are employed. This study is a continuation of the paper by Molcard et al. (2009). In response to the four questions posed in Section 1, we can provide the following answers based on the analysis above.

This small-scale coastal flow from VHF radar indicates complex LCS fields estimated using the FSLE. We find that there is a very good agreement between the spatial and temporal evolution of the FSLE fields

and the motion of the drifter clusters. In particular, the drifters follow but do not cross the FSLE ridges, thus confirming that the FSLE ridges act as natural transport barriers in the flow field. The FSLE seems to be an effective tool in mapping the natural transport barriers of the flow field.

The surface flow in the Gulf of La Spezia appears to be mainly forced by the ambient circulation in the Ligurian Sea, which sets the large-scale deformation field. We also find some evidence of strong modulation of the surface current by the local wind forcing as well as inertial oscillations. The wavenumber spectrum is limited by the small size of the domain (5 to 10 km) and radar resolution (250 m). The spectrum shows peaks of energy straddling 1 km, which is close to the Rossby radius of deformation. Nevertheless, the Rossby number $Ro \approx 1$ is large enough for rotational effects not to be dominant. Formation of isolated eddies is not observed either because of large Ro and/or the proximity of the domain size to R_d . Both the overall level and the distribution of energy among different wavenumbers are highly time dependent, indicating that the spectrum is dominated by individual events and external forcing, as opposed to a well-established steady energy cascade which is characteristic of the breakdown of isolated coherent structures into smaller-scale eddies.

It is found that the FSLE $\lambda(\delta)$ is nearly scale independent for the spatial scale range of 0.1125 m to 1–2 km, varying within a range of $\lambda \approx 4 \text{ day}^{-1}$ and $\lambda \approx 7 \text{ day}^{-1}$. Since the observational area of the radar essentially corresponds to the submesoscale range, the relative dispersion in the mesoscale range and beyond is not quantified. Computation of $D^2(t)$ supports this exponential or nonlocal regime and value of λ . Therefore, there are no indications of significant control by rapidly evolving, small-scale turbulent features on the

relative dispersion. The computed FSLE range is more than an order of magnitude larger than those found from modeling results by Haza et al. (2008) and Poje et al. (2010) and the observational value obtained by LaCasce and Ohlmann (2003) based on SCULP data in the Gulf of Mexico, but somewhat smaller than the limiting value put forward by Lumpkin and Ellipot (2010) from CLIMODE drifters in the Gulf Stream. We also find that scaling the limiting value of the FSLE by the resolved gradients of the Eulerian fields as given by a positive Okubo–Weiss criterion is useful, and the linear fit to data from Poje et al. (2010) almost extends to the flows considered here.

The horizontal flow convergence is seen to have a small yet tangible effect on relative dispersion in this study. Nevertheless, given that the radar resolution of 250 m is at the high end of persistent phenomena such as Langmuir cells and our relative dispersion study relies on synthetic rather than real drifters, we are unable to address this matter further at this stage.

A number of important steps remain to be explored in future studies. The first is that, while we found a good correspondence between the pattern of manifolds from the FSLE computations and the motions of drifters in the two clusters, the number of drifters and clusters employed here are small, thus far from providing total insight on the utility of dynamical systems approaches for oceanic transport. This study highlights not only the need of simultaneous release of large drifter clusters consisting of pairs of triplets but also the simultaneous use of independent (Eulerian/Lagrangian) measurements in future observing systems. The combination of coastal VHF radars and surface drifters appears to provide independent and complementary data sets which seem extremely useful to explore transport processes at the submesoscale range. Given the recent proliferation of coastal radars and reduction in cost of surface drifters with GPS sampling, similar studies should be pursued at different geographical locations in order to develop a better understanding of the nature of coastal transport. Second, all our existing results indicate a clear exponential regime at scales smaller than the radius of deformation, pointing toward nonlocal dynamics (Fig. 14). Given limited modeling and observational capabilities, these should be viewed as suggestive results. In order to attain a better understanding of oceanic turbulence and transport, it would be of great interest to find out under which circumstances (dynamics and/or forcing) the local regime emerges. This, again, points toward the need of studies with more comprehensive observing systems and using highly resolved models with comprehensive dynamics and/or forcing. Third, with the sampling of smaller scales

along the coastal ocean with complex bathymetry, shallow waters, and wind forcing, the effect of horizontal flow divergence on relative dispersion deserves more attention. In particular, the implications of using 2-D drifters in a flow that may show 3-D patterns needs to be investigated. Finally, studies using 3-D Lagrangian transport and corresponding development in theory should be pursued.

Acknowledgements We are grateful to ONR via grants N00014-05-1-0094 and N00014-05-1-0095 (Haza, Özgökmen, Griffa), N00014-08-2-1146 and N00173-07-2-C901 (Peggion), and to EC through the ECOOP project (Griffa). We wish to acknowledge the contribution from the NRL scientific team with special thanks to Dr. C. Rowley and Mr. R. Allard and Dr E. Coelho. We also thank A. Lisca for sharing the data from the ENEA meteorological station.

References

- Aref H (1984) Stirring by chaotic advection. *J Fluid Mech* 192:115–173
- Artale V, Boffetta G, Celani A, Cencini M, Vulpiani A (1997) Dispersion of passive tracers in closed basins: beyond the diffusion coefficient. *Phys Fluids* 9:3162–3171
- Astraldi M, Gasparini G, Manzella G (1990) Temporal variability of currents in the eastern Ligurian Sea. *J Geophys Res* 95(C2):1515–1522
- Aurell E, Boffetta G, Crisanti A, Paladin G, Vulpiani A (1997) Predictability in the large: an extension of the concept of Lyapunov exponent. *J Phys A* 30:1–26
- Barbin Y, Broche P, de Maistre J-C, Forget P, Gaggelli J (2006) Practical results of direction finding method applied on a 4 antenna linear array WERA. ROW-6 Radiowave Oceanography Workshop
- Barrick D, Lipa BJ (1986) The second-order shallow water hydrodynamic coupling coefficient in interpretation of HF radar sea echo. *IEEE J Oceanic Eng OE-11*:310–315
- Bauer S, Swenson M, Griffa A (2002) Eddy mean flow decomposition and eddy diffusivity estimates in the tropical Pacific Ocean: 2. Results. *J Geophys Res* 107:C10. doi: [10.1029/2000JC000613](https://doi.org/10.1029/2000JC000613)
- Bennett AF (1984) Relative dispersion—local and nonlocal dynamics. *J Atmos Sci* 41(11):1881–1886
- Berloff P, McWilliams J (2002) Material transport in oceanic gyres. Part 2: hierarchy of stochastic models. *J Phys Oceanogr* 32/3:797–830
- Boccaletti G, Ferrari R, Fox-Kemper B (2007) Mixed layer instabilities and restratification. *J Phys Oceanogr* 37:2228–2250
- Bordone A, Lisca A (2009) Meteorological data from the ENEA station of S.Teresa (sp). RT ENEA/2009/15/ACS
- Broche P, Barbin Y, De Maistre J-C, Forget P, Gaggelli J (2004) Antennas processing and design for VHF COSMER coastal radar. ROW-4 Radiowave Oceanography Workshop
- Castellari S, Griffa A, Özgökmen T, Poulain P-M (2001) Prediction of particle trajectories in the Adriatic Sea using Lagrangian data assimilation. *J Mar Syst* 29:33–50
- Coulliette C, Wiggins S (2000) Intergyre transport in a wind-driven, quasigeostrophic double gyre: an application of lobe dynamics. *Nonlinear Process Geophys* 7:59–85

- Craik A, Leibovich S (1976) A rational model for Langmuir circulations. *J Fluid Mech* 73:401–426
- Davis R (1985) Drifter observations of coastal currents during CODE. The method and descriptive view. *J Geophys Res* 90:4741–4755
- Davis R (1991) Observing the general-circulation with floats. *Deep-Sea Res* 38:531–571
- d'Ovidio F, Fernandez V, Hernandez-Garcia E, Lopez C (2004) Mixing structures in the Mediterranean Sea from finite-size Lyapunov exponents. *Geophys Res Lett* 31:L17203. doi:10.1029/2004GL020328
- Essen H-H, Gurgel K-W, Schlick T (2000) On the accuracy of current measurements by means of HF radar. *IEEE J Oceanic Eng* 25:472–480
- Falco P, Griffa A, Poulain P, Zambianchi E (2000) Transport properties in the Adriatic Sea as deduced from drifter data. *J Phys Oceanogr* 30:2055–2071
- Fratantoni D (2001) North Atlantic surface circulation during the 1990's observed with satellite-tracked drifters. *J Geophys Res* 106:22067–22093
- Gasparini G, Abbate M, Bordone A, Cerrati G, Galli C, Lazzoni E, Negri A (2009) Circulation and biomass distribution during warm season in the Gulf of La Spezia (north-western Mediterranean). *J Mar Syst* 78/1:S48–S62
- Griffa A (1996) Applications of stochastic particle models to oceanographic problems. In: Adler R, Müller P, Rozovskii B (eds) *Stochastic modelling in physical oceanography*, vol 467. Birkhauser, Boston, pp 113–128
- Griffa A, Lumpkin R, Veneziani M (2008) Cyclonic and anticyclonic motion in the upper ocean. *Geophys Res Lett* 35:L01608. doi:10.1029/2007GL032100
- Gurgel K-W, Antonischki G, Essen H-H, Schlick T (1999) Weller radar (WERA): a new ground wave radar for remote sensing. *Coast Eng* 37:219–234
- Haller G (1997) Distinguished material surfaces and coherent structures in three-dimensional flows. *Physica D* 149/4:248–277
- Haller G, Poje A (1998) Finite time transport in aperiodic flows. *Physica D* 119:352–380
- Haza AC, Griffa A, Martin P, Molcard A, Özgökmen TM, Poje AC, Barbanti R, Book JW, Poulain PM, Rixen M, Zanasca P (2007) Model-based directed drifter launches in the Adriatic Sea: results from the DART experiment. *Geophys Res Lett* 34:L10605. doi:10.1029/2007GL029634
- Haza AC, Poje A, Özgökmen TM, Martin P (2008) Relative dispersion from a high-resolution coastal model of the Adriatic Sea. *Ocean Model* 22:48–65
- Kaplan D, Largier J, Botsford L (2005) HF radar observations of surface circulation off Bodega Bay (northern California, USA). *J Geophys Res* 110:C10020. doi:10.1029/2005JC002959
- LaCasce J, Bower A (2000) Relative dispersion in the subsurface North Atlantic. *J Mar Res* 58:863–894
- LaCasce JH, Ohlmann C (2003) Relative dispersion at the surface of the Gulf of Mexico. *J Mar Res* 61(3):285–312
- Lacorata G, Aurell E, Vulpiani A (2001) Drifter dispersion in the Adriatic Sea: Lagrangian data and chaotic model. *Ann Geophys* 19:121–129
- Langmuir I (1938) Surface motion of water induced by wind. *Science* 41:119–123
- Lesieur M (1997) Turbulence in fluids. In: *Fluid mechanics and its applications*, vol 40. Kluwer Academic, Amsterdam
- Lumpkin R, Ellipot S (2010) Surface drifter pair spreading in the North Atlantic. *J Geophys Res* (in press)
- Mahadevan A (2006) Modeling vertical motion at ocean fronts: are nonhydrostatic effects relevant at submesoscales? *Ocean Model* 14:222–240
- Martin PJ (2000) Description of the navy coastal ocean model version 1.0. Naval Research Laboratory report, RL/FR/7322-00-9962, 42 pp
- McWilliams JC (1985) Submesoscale, coherent vortices in the ocean. *Rev Geophys* 23(2):165–182
- McWilliams JC (2003) Diagnostic force balance and its limits. In: *Nonlin. proc. geophys. fluid dyn.*, pp 287–304
- Miller P, Pratt L, Helfrich K, Jones C (2002) Chaotic transport of mass and potential vorticity for an island recirculation. *J Phys Oceanogr* 32:80–102
- Molcard A, Poje A, Özgökmen T (2006) Directed drifter launch strategies for Lagrangian data assimilation using hyperbolic trajectories. *Ocean Model* 12:268–289
- Molcard A, Poulain P, Forget P, Griffa A, Barbin Y, Gaggeli J, Maistre JD, Rixen M (2009) Comparison between VHF radar observations and data from drifter clusters in the Gulf of La Spezia (Mediterranean Sea). *J Mar Syst* 78/1:S78–S89
- Molemaker M, McWilliams J (2005) Baroclinic instability and loss of balance. *J Phys Oceanogr* 35:1505–1517
- Ohlmann C, White P, Washburn L, Terrill E, Emery B, Otero M (2007) Interpretation of coastal HF radar-derived surface currents with high-resolution drifter data. *J Atmos Ocean Technol* 24/4:666–680
- Okubo A (1970) Horizontal dispersion of floatable particles in vicinity of velocity singularities such as convergences. *Deep-Sea Res* 17(3):445–454
- Olascoaga M, Rypina II, Brown MG, Beron-Vera FJ, Kocak H, Brand LE, Halliwell GR, Shay LK (2006) Persistent transport barrier on the West Florida Shelf. *Geophys Res Lett* 33:22603. doi:10.1029/2006GL027800
- Ottino J (1989) *The kinematics of mixing: stretching, chaos and transport*. Cambridge University Press, Cambridge
- Özgökmen T, Griffa A, Piterbarg L, Mariano A (2000) On the predictability of Lagrangian trajectories in the ocean. *J Atmos Ocean Technol* 17:366–383
- Özgökmen T, Piterbarg L, Mariano A, Ryan E (2001) Predictability of drifter trajectories in the tropical Pacific Ocean. *J Phys Oceanogr* 31:2691–2720
- Paduan J, Kim K, Cook M, Chavez F (2006) Calibration and validation of direction finding high frequency radar ocean current observations. *IEEE J Oceanic Eng* 31(4):862–875. doi:10.1109/JOE.2006.886195
- Paduan J, Rosenfeld L (1996) Remotely sensed surface currents in Monterey Bay from shore based HF radar (Coastal ocean dynamics application radar). *J Geophys Res* 101/C9:20669–20686
- Poje A, Haller GG (1999) Geometry of cross-stream mixing in a double-gyre ocean model. *J Phys Oceanogr* 29:1649–1665
- Poje A, Haza A, Özgökmen T, Magaldi M, Garraffo Z (2010) Resolution dependent relative dispersion statistics in a hierarchy of ocean models. *Ocean Model* 31:36–50
- Poje AC, Toner M, Kirwan AD, Jones CKRT (2002) Drifter launch strategies based on Lagrangian templates. *J Phys Oceanogr* 32:1855–1869
- Poulain P-M (1999) Drifter observations of surface circulation in the Adriatic Sea between December 1994 and March 1996. *J Mar Syst* 20:231–253
- Richardson P (2001) Drifters and floats. In: *Encyclopedia of ocean studies*, vol 2, pp 767–774
- Schott F, Frisch S, Larsen J (1986) Comparison of surface currents measured by HF Doppler Radar in the western Florida

- Straits during November 1983 to January 1984 and Florida Current transport. *J Geophys Res* 91:8451–8460
- Shadden S, Lekien F, Paduan JD, Chavez FC, Marsden JE (2008) The correlation between surface drifters and coherent structures based on high-frequency data in Monterey Bay. *Deep-Sea Res II* 56:161–172
- Shay L, Lentz S, Graber H, Haus B (1998a) Current structure variations detected by high frequency radar and vector measuring current meters. *J Atmos Ocean Technol* 15:237–256
- Shay L, Lee T, Williams E, Graber H, Rooth C (1998b) Effects of low frequency current variability on submesoscale near-inertial vortices. *J Geophys Res* 103:18691–18714
- Shay L, Cook T, Hallock Z, Haus B, Graber H, Martinez J (2001) The strength of the M2 tide at the Chesapeake Bay mouth. *J Phys Oceanogr* 31:427–449
- Shay L, Martinez-Pedraja J, Cook T, Haus B (2007) High-frequency radar mapping of surface currents using WERA. *J Atmos Ocean Technol* 24:484–503
- Skillingstad ED, Denbo D (1995) An ocean large-eddy simulation of Langmuir circulations and convection in the surface mixed layer. *J Geophys Res* 100:8501–8522
- Steward R, Joy J (1974) HF radio measurements of surface currents. *Deep-Sea Res* 21:1039–1049
- Thomas LN, Tandon A, Mahadevan A (2008) Sub-mesoscale processes and dynamics. In Hecht MW, Hasumi H (eds) *Ocean modeling in an eddying regime*, geophysical monograph series, vol 177. American Geophysical Union, Washington DC, pp 17–38
- Toner M, Poje AC (2004) Lagrangian velocity statistics of directed launch strategies in a Gulf of Mexico model. *Nonlinear Process Geophys* 11:35–46
- Ullman D, O'Donnell J, Kohut J, Fake T, Allen A (2006) Trajectory prediction using HF radar surface currents: Monte Carlo simulations of prediction uncertainties. *J Geophys Res* 111:C12005. doi:10.1029/2006JC003715
- Vandenbulcke L, Beckers J, Lenartz F, Barth A, Poulain P, Aidonidis M, Meyrat J, Ardhuin F, Tonani M, Fratianni C, Torrisi L, Pallela D, Chiggiato J, Tudor M, Book JW, Martin P, Peggion G, Rixen M (2009) Super-ensemble techniques: application to surface drift prediction during the DART06 and MREA07 campaigns. *Prog Oceanogr* 82:149–167
- Veneziani M, Griffa A, Garraffo Z, Chassignet E (2005a) Lagrangian spin parameter and coherent structures from trajectories released in a high-resolution ocean model. *J Mar Res* 63/4:753–788
- Veneziani M, Griffa A, Reynolds A, Garraffo Z, Chassignet E (2005b) Parameterizations of Lagrangian spin statistics and particle dispersion in the presence of coherent vortices. *J Mar Res* 63/6:1057–1083
- Weiss J (1991) The dynamics of enstrophy transfer in 2-dimensional hydrodynamics. *Physica D* 48(2–3):273–294
- Weller R, Price J (1988) Langmuir circulation within the oceanic mixed layer. *Deep-Sea Res* 35:711–747
- Wiggins S (2005) The dynamical systems approach to Lagrangian transport in oceanic flows. *Ann Rev Fluid Mech* 37:295–328